ECOLOGY

Land change, fire, and climate weaken carbon sink in the conterminous United States

Jinxun Liu[1]*, Benjamin M. Sleeter[1], Zhiliang Zhu[1], Mark A. Cochrane[2], Qiang Zhou[3], Bin Wang[4], Grant M. Domke[5], Paul C. Selmants[1], Lisamarie Windham-Myers[1], Qiuan Zhu[6], Tamara S. Wilson[1], Kristin B. Byrd[1], Eric J. Ward[7,8], Terry L. Sohl[1], Todd J. Hawbaker[1], Zhen Zhang[9], Christopher E. Soulard[1], Kimberly P. Wickland[1], Robert G. Striegl[1]

The land carbon sink of the conterminous United States was evaluated using a bottom-up modeling framework and 30-meter land change data from 1985 to 2020. This cross-scale, cross-landscape, and cross-system approach tracked fractional land cover changes and applied regional model calibration. Results show average terrestrial and aquatic carbon sinks of +110 ± 37 and +19 ± 0.5 teragrams of carbon per year, respectively. The terrestrial carbon sink, showing no clear trend, peaked in the 1990s, with more years as a carbon source since 2000, contradicting recent national and global studies. Land change had the largest impact (−70 ± 5.5 teragrams of carbon per year), exceeding impacts of climate (−33 ± 48 teragrams of carbon per year), wildfire (−7.7 ± 2.4 teragrams of carbon per year), and erosion transport (−1.9 ± 0.13 teragrams of carbon per year). The positive CO_2 fertilization effect (+69 ± 12 teragrams of carbon per year) was insufficient to maintain the carbon sink strength. Our framework reveals key paths of carbon loss, with implications for carbon budget and energy policies in the United States and beyond.

INTRODUCTION

Globally, the terrestrial land surface, including wetlands and inland water systems, provide a substantial sink for atmospheric carbon (C), absorbing roughly 38% of all anthropogenic emissions annually (*1*). Land C sink, the net annual C sequestration rate, is strongly related to human land use activities, climate, natural disturbances, and atmospheric CO_2 increases. However, the quantification of land C sink is so diverse and sometimes controversial (*1–3*) that scientists have put forward an integrative framework to better quantify the land C sink, including understanding the linkage between terrestrial and aquatic systems and the gap between atmospheric-based ("top-down") and land-based ("bottom-up") C estimates (*4*, *5*).

Recent global studies informed by atmospheric inversion models, dynamic global vegetation models (DGVMs), and inventory analyses indicate that land C sink strength has been increasing or steady over the several past decades (*1*, *6*, *7*). However, other studies like the Intergovernmental Panel on Climate Change Sixth Assessment Report (*8*) indicate that severe impacts of global warming on high-C ecosystems have already led to a weakening C sink. For North America and the conterminous United States (CONUS), both the Regional Carbon Cycle Assessment and Processes–2 (RECCAP2) synthesis (*5*) and the US Second State of the Carbon Cycle Report (SOCCR2) (*9*) estimate that combined atmospheric measurements, models, and land inventories indicate no consistent increasing or decreasing trends in land C sink strength around 2010s. Conversely, the US National Greenhouse Gas Inventory estimates for the forest land category, which are largely based on the Nationwide Forest Inventory (NFI), show declining sink strength since 1990 with substantial interannual variability (*10*).

Overall, estimates of global and regional terrestrial C sink vary widely and are highly dependent on input data and methodology. Recent research indicates that remote sensing–based global C sink estimates are lower by a factor of 3 than the Coupled Model Intercomparison Project phase 6 (CMIP6) model results (*11*). Terrestrial C sink estimates for CONUS range from ~200 to 685 Tg C year^{-1}, with field inventory estimates at the lower end, atmospheric inversion estimates at the higher end, and other modeling estimates in between (*2*).

Highly variable land C sink estimates are expected because land C dynamics are complex and controlled by many interacting factors, including atmospheric chemistry, climate, natural disturbance, human land use, vegetation succession, and cross-landscape C transports. Land C sink estimates constrained by or derived from atmospheric inversion are top-down modeling results that usually do not consider land change processes, and any errors in atmospheric and ocean C budgets will directly propagate into top-down estimates of the land C sink (*3*, *12*). A recent study indicates that the global ocean C sink has been underestimated (*13*), implying that previous global land C sinks could be overestimated. However, regional C sink variabilities are complex. Tropical Amazon could be experiencing weakening land C sink due to large-scale deforestation, while East Asia could be enhancing land C sink due to massive afforestation (*14*, *15*). North America may have a unique C sink texture mixed with forest management, climate variability, wildfire, drought, pest outbreak, urbanization, and ecosystem aging. Therefore, a bottom-up C sink quantification is needed to reveal the CONUS land C cycle details.

Land C sinks derived from eddy-covariance flux tower measurements are bottom-up results, but because of their small C flux footprints, flux tower measurements cannot capture extensive regional land disturbance events such as wildfire, deforestation, and

[1]US Geological Survey, Reston, VA 20192, USA. [2]University of Maryland Center for Environmental Science (UMCES), Cambridge, MD 21613, USA. [3]Science Systems and Applications, Inc (SSAI), contractor to NASA GSFC, Pueblo, CO 81001, USA. [4]Computational Sciences and Engineering Division, Oak Ridge National Laboratory, Oak Ridge, TN 37831, USA. [5]USDA Forest Service, Washington, DC 20250, USA. [6]Hohai University, Nanjing, Jiangsu 210098, China. [7]Earth System Science Interdisciplinary Center, University of Maryland, College Park, MD 20740, USA. [8]Biospheric Sciences Laboratory, NASA Goddard Space Flight Center, Greenbelt, MD 20771, USA. [9]Institute of Tibetan Plateau Research, Chinese Academy of Sciences, Beijing 100101, China.
*Corresponding author. Email: jxliu@usgs.gov

urbanization. Also, the range of vegetation types, plant species, and stand conditions at flux tower sites are typically narrow and do not fully represent regional vegetation conditions. In particular, reginal average growth rate and mortality rate could be different from site-scale observations. In contrast, the NFI in the United States is a spatially representative, probability sample with remeasurements every 5 to 10 years on permanent plots across all land ownerships. These data are used to compile population estimates of forest C stocks and changes across scales (e.g., county to national) (*10*, *16*).

DGVMs are process-based bottom-up approaches often used to evaluate C trends and differentiate driver impacts, which are independent from inversions and extend beyond local scales. However, previous national and global-scale coarse spatial resolution DGVM studies (*17*) were unable to incorporate detailed land use and land cover change (LUCC) either due to model structure or lack of observed land change data. The widely used modeled GLM2-HYDE (*18*) data for the CMIP5/CMIP6 models only provides net land change rates at a coarse resolution (0.25°), missing gross or total land conversions that substantially affect C calculation. For example, if a land cell experiences both deforestation and an equal amount of reforestation, the net change in forest cover fraction will be zero, and the C sink could be miscalculated if no forest change is assumed. Furthermore, many previous DGVM modeling studies did not incorporate harvest, lateral C movement across the landscape, or C transport across the terrestrial-aquatic continuum (*9*, *17*).

Cross-scale, cross-landscape, and cross-system considerations could help improve confidence in regional and global estimates of land surface C estimates. Here, cross-scale C modeling means using high spatial resolution (30 m) wall-to-wall remote-sensing observation series to capture detailed land change history over large regions (i.e., CONUS) and using regional (county/ecoregion) C data for model calibration. This approach uniquely distinguishes cross-scale C estimates from coarse-resolution atmospheric inversion estimates and estimates derived from interpolating local-scale eddy flux tower measurements or field inventories. Adding remotely sensed land change processes such as fractional land cover change and wildfire burn severity levels in DGVM allows accurate C accounting that coarse-resolution models (without remote sensing data) and site-scale data (missing regional-scale C feature or parameters) would be hard to achieve.

Cross-scale studies also include lateral C transport processes often overlooked in other studies. Soil C transport across landscapes and from inland to coastal regions is a critical component in the overall C cycle that is currently missing from most models (*19*). In addition, organic C leaching from soil profile and inorganic C yield from biologic and geologic sources also put a substantial amount of C into the aquatic systems (*20*). Incorporating these cross-landscape and cross-system C processes in land C sink estimates, together with detailed land change considerations, increases the accuracy and attribution of the land C fluxes.

The flexibility of DGVMs in spatial and temporal scopes and explainability in terms of driver impacts on C stocks and fluxes make them well suited for cross-scale, cross-landscape, and cross-system process modeling. However, using high-resolution (e.g., ≤30 m) remote-sensing products to constrain C estimates in DGVMs can be challenging (*21*). Missing land change processes need to be added in these models. High-resolution land change data need to be aggregated to coarser resolutions (e.g., 1 to 10 km) that DGVMs can handle as mixed land pixels, with major land conversions represented as subpixel level fractional changes (*2*). In addition, substantial effort is needed to port high-resolution DGVMs to advanced computing resources (e.g., exascale supercomputers), pushing the boundaries of modeling technology in data and computational scalability.

We developed the parallel-computing version of the Integrated Biosphere Simulator (pIBIS) (*2*, *22*), a process-based DGVM, to access terrestrial and inland water C sinks in the CONUS at 1-km resolution from 1985 to 2020. We enhanced the model to incorporate fine-resolution land cover change data over large regions, account for a broader range of land cover conversions, and track fractional land cover changes. Furthermore, we integrated additional components to simulate lateral C transport across landscapes and from terrestrial to aquatic systems, which further linked to an offline inland water C accounting model.

We chose 1-km resolution in this study because we are using 30-m remote-sensing data that DGVMs cannot handle. The 1-km resolution is likely the upper limit for DGVMs to use current supercomputing resources. We evaluated terrestrial C sinks in drylands, wetlands, and coastal tidal mudflats, and accounted for aquatic C sinks through C burial in inland water bodies. Details are provided in Materials and Methods.

Landsat-based 30-m Land Change Monitoring, Assessment, and Projection (LCMAP) data and data from the Monitoring Trends in Burn Severity (MTBS) were aggregated to 1 km (990 m) to assess fractional land change and fire disturbance. Our objectives were to estimate the recent land C budget for the CONUS from 1985 to 2020 and analyze its responses to CO_2 fertilization, LUCC, climate variability, wildfire, and lateral C transport. We simulated ecosystem net primary productivity (NPP, annual biomass growth), net ecosystem productivity (NEP, equal to NPP minus heterotrophic respiration from soil and litter), and net biome productivity (NBP, equal to NEP minus C losses from fire, LUCC, leaching and erosion, i.e., the net terrestrial C sink) of forest, shrub, grass, agricultural lands, and wetlands.

We used the Unit Stream Power–based Erosion Deposition model (USPED) (*23*) to quantify soil erosion and deposition (ED) across CONUS at 90-m resolution and then derive soil C ED in pIBIS. We also added a nonspatial inland water C spreadsheet model based on spatially explicit terrestrial leaching, ED, and a partial inversion from previous aquatic C studies (*9*, *20*). Model calibration was based on county-scale numbers from forest field inventories, agricultural census data, and remote sensing products (*2*). The current model does not incorporate C accounting for harvested wood products and landfills.

Five simulation scenarios were used to analyze the individual effects of CO_2 fertilization, climate change, wildfire, and LUCC on C flux and stock changes, including

1. The Climate-CO_2 reference scenario used dynamic climate and CO_2 data from 1985 to 2020 but excluded LUCC and fire effects.
2. The Fire scenario incorporated wildfire into the Climate-CO_2 scenario.
3. The LUCC-Fire scenario incorporated both LUCC and fire into the Climate-CO_2 scenario.
4. The No-Climate-Change scenario removed dynamic climate data from the Climate-CO_2 scenario and instead used climate data from 1976 to 1985, representing an average pre-1985 climate condition. For each year between 1986 and 2020, a year was randomly selected from the 1976–1985 period, and its climate data were applied.
5. The No-CO_2-Increase scenario removed increasing atmospheric CO_2 data from the Climate-CO_2 scenario and used a fixed 1985 atmospheric CO_2 concentration [346 parts per million (ppm)].

RESULTS

Land-aquatic C stocks and fluxes of CONUS

Total land-aquatic NBP is the sum of all C fluxes among the five C pools (live biomass, litter, dead wood, soil, and inland water) as shown in Fig. 1. The arrows indicate C fluxes into or out of related C pools. C amounts leaving the land-aquatic system (to atmosphere and ocean) are marked as negative (−) values. For each C pool, net C change equals in-flux minus out-flux. On land pixel-scale, disposition C is an in-flux while erosion C is an out-flux.

The total land C sink (terrestrial + aquatic) averaged 130 ± 37 Tg C year^{-1} from 1985 to 2020, without considering C sink in landfills and harvested wood products. CONUS-scale C stocks and fluxes are illustrated in Fig. 1. A streamlined decadal summary is presented in Table 1. More detailed C stock and flux information are provided in the Supplementary Materials. On the basis of trendline from 1985 to 2020, terrestrial NPP, NEP, and heterotrophic respiration increased by 19.8 ± 0.3, 26.6 ± 3.2, and 16.6 ± 1.0%, respectively. However, terrestrial NBP, the net terrestrial C sink after land use, fire, and erosion, did not show an increasing trend and averaged 110 ± 37 Tg C year^{-1}. For terrestrial C sink, not including aquatic C burial, CONUS acted as a C source in 1988, 2001, 2002, 2006, 2007, 2012, and 2018. C stocks of live biomass, deadwood, litter, and soil organic C increased by 6.4 ± 4.3, 32.0 ± 4.6, 8.1 ± 0.9, and 1.7 ± 0.3%, respectively.

Excluding soil respiration, the total organic C removed from terrestrial ecosystems averaged −700 ± 21 Tg C year^{-1}, including agricultural harvest (−480 ± 2.7 Tg C year^{-1}), LUCC (−180 ± 20 Tg C year^{-1}), leaching (−30 ± 1.2 Tg C year^{-1}), wildfire (−9.4 ± 1.8 Tg C year^{-1}), and erosion (−8.8 ± 0.3 Tg C year^{-1}). LUCC-induced and wildfire-related C losses were −170 ± 18 and −3.9 ± 1.1 Tg C year^{-1} from 1985 to 2000, increasing to −180 ± 22 and −13.7 ± 2.3 Tg C year^{-1} from 2001 to 2020, respectively, reflecting ~10 and ~350% increases. The wildfire C loss in 2020 alone reached −48 ± 9.7 Tg C year^{-1}.

Total terrestrial to aquatic organic C transfer included leaching (30.4 ± 1.2 Tg C year^{-1}) and erosion (8.8 ± 0.3 Tg C year^{-1}), which were counted as C losses (outputs) from the terrestrial systems but gains (inputs) of the aquatic systems. On the basis of trendline analysis, the leaching C increased by 45.5 ± 2.3%, while erosion C increased by 18.0 ± 0.9% during the study period. A partial inversion amount of dissolved inorganic C (DIC) from terrestrial biologic sources (49 ± 1.8 Tg C year^{-1}, a portion from soil CO_2 release) and geologic sources (49 ± 1.1 Tg C year^{-1}) were included as input to aquatic system. Urban releases (1.0 Tg C year^{-1}) were also added. Conversely, 2.0 Tg C year^{-1} were deposited from aquatic systems to coastal mudflats and tidal wetlands where elevations were less than 2 m and terrain slopes were zero.

For the period 1991–2010, CONUS terrestrial NBP averaged 128 Tg C year^{-1}. After accounting for the Harvested Wood Product C sink, approximately 25 Tg C year^{-1} (*2*), the adjusted average NBP was 153 Tg C year^{-1}. This value is about 24% lower than previous pIBIS C sink estimates (*2*) and 45% lower than SOCCR2 estimates (*9*). The total C sink (terrestrial + aquatic) for the 2011–2020 period (123 Tg C year^{-1}) is approximately 38% lower than the recent DGVM synthesis (*17*), which estimated 170 Tg C year^{-1}.

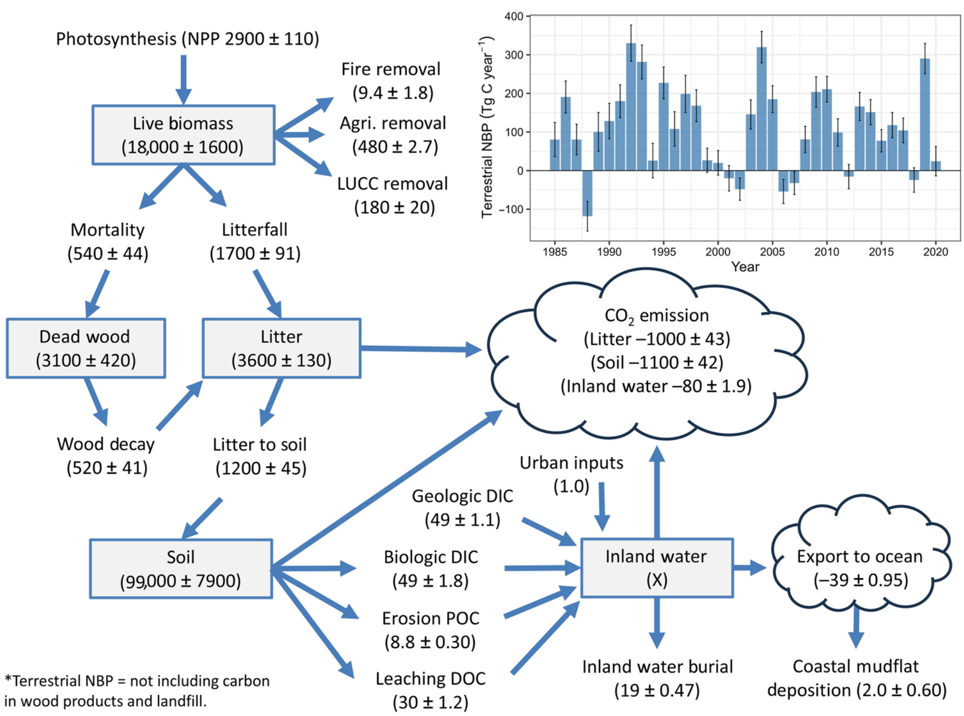

Fig. 1. Ecosystem C stocks and fluxes of the conterminous United States from 1985 to 2020. (i) Values in the flowchart represent the 1985 to 2020 annual mean C stock or flux with uncertainty ranges (units in teragrams of carbon and teragrams of carbon per year). The C stock of inland waters is unknown but assumed to be constant. NPP, net primary productivity; NBP, net biome productivity; DIC, dissolved inorganic carbon; DOC, dissolved organic carbon; POC, particulate organic carbon. (ii) The inset graph shows the temporal trends of CONUS-scale terrestrial NBP, with uncertainty range (1.96 x STDEV) based on Monte Carlo simulations. A positive value indicates net C gain, while negative value indicates net C loss.

Table 1. Ecosystem productivities, C stocks, and C fluxes in the conterminous United States. Values are of different C categories but rounded off to two reliable digits. Uncertainty range is at 95% confidence level (1.96 * SD) based on 40 Monte Carlo simulations.

	1985–1990	1991–2000	2001–2010	2011–2020	1985–2020
Terrestrial NPP (Tg C year^{-1})	2700 ± 100	2900 ± 110	2900 ± 110	3200 ± 120	2900 ± 110
Terrestrial NEP (Tg C year^{-1})	660 ± 56	790 ± 56	780 ± 51	850 ± 53	780 ± 54
Terrestrial NBP (Tg C year^{-1})	80 ± 42	160 ± 41	99 ± 34	99 ± 33	110 ± 37
Live biomass (Tg C)	18000 ± 1300	18000 ± 1500	18000 ± 1600	19000 ± 1800	18000 ± 1600
Deadwood (Tg C)	2800 ± 370	3000 ± 400	3200 ± 430	3400 ± 460	3100 ± 420
All litter (Tg C)	3500 ± 120	3600 ± 130	3600 ± 140	3700 ± 140	3600 ± 130
Soil carbon (Tg C)	98000 ± 7900	98000 ± 7900	99000 ± 7900	99000 ± 7900	99000 ± 7900
Leaching (Tg C year^{-1})	24 ± 1.0	30 ± 1.2	29 ± 1.2	36 ± 1.5	30 ± 1.2
Erosion (Tg C year^{-1})	8.2 ± 0.30	8.7 ± 0.30	8.7 ± 0.40	9.5 ± 0.40	8.8 ± 0.30
DIC_geo (Tg C year^{-1})	40 ± 1.0	49 ± 1.1	45 ± 1.1	60 ± 1.2	49 ± 1.1
DIC_bio (Tg C year^{-1})	36 ± 1.4	47 ± 1.7	45 ± 1.7	64 ± 2.3	49 ± 1.8
LUCC C loss (Tg C year^{-1})	160 ± 17	170 ± 18	180 ± 21	190 ± 22	180 ± 20
Fire C loss (Tg C year^{-1})	4.4 ± 1.0	3.6 ± 1.1	8.6 ± 1.2	19 ± 3.4	9.4 ± 1.8
Agri. harvest (Tg C year^{-1})	410 ± 2.4	450 ± 2.5	480 ± 3.0	530 ± 2.6	480 ± 2.7
Aquatic C burial (Tg C year^{-1})	15 ± 0.40	19 ± 0.50	18 ± 0.40	24 ± 0.60	19 ± 0.50
Aquatic C export (Tg C year^{-1})	31 ± 0.80	38 ± 0.90	36 ± 0.90	48 ± 1.1	39 ± 0.90

C stock by scenarios and trends of NPP and NEP under the Climate-CO_2 scenario

Biomass and soil C stocks under different simulation scenarios are shown in Fig. 2 (A to C). All scenarios indicate that C stocks increased from 1985 to 2020. Similarly, ecosystem NPP, NEP, and soil respiration overall increased, although the changes varied spatially (Fig. 2, D to F).

The LUCC-Fire and Fire scenarios had lower estimates of biomass and soil C stocks when compared with the Climate-CO_2 scenario, with LUCC showing a much bigger negative impact than Fire. The No-Climate-Change scenario yielded the highest biomass and soil C estimates of all scenarios, indicating that changing climate had a negative effect on C sink. The No-CO_2-Increase scenario had the lowest soil C stock and the second lowest biomass stock, indicating that CO_2 fertilization had larger positive effect on soil C than other factors. However, climate also substantially affected soil C in later years.

The Climate-CO_2 simulation represents an ecosystem natural succession scenario. The regression slopes of NPP, NEP, and soil respiration over time for each land pixel indicate that their pixel level trends from 1985 to 2020 (Fig. 2 (D to F). In general, NPP increased in eastern CONUS and was relatively stable or slightly decreased in the west. However, NEP of eastern forests did not notably increase, and NEP of some western forest locations decreased. Soil respiration increased in most forest areas in the eastern CONUS and West Coast (Fig. 2F).

Effects of CO_2 fertilization, climate change, LUCC and wildfire on C stock and flux

We quantified the impacts of climate, LUCC, wildfire, erosion, and CO_2 fertilization on land C sink strength by further analyzing differences among the scenarios. LUCC had the greatest negative impact on C sink strength (−70 ± 5.5 Tg C year^{-1}), exceeding the impacts of climate (−33 ± 48 Tg C year^{-1}), wildfire (−7.7 ± 2.4 Tg C year^{-1}), and erosion transport (−1.9 ± 0.13 Tg C year^{-1}). The positive CO_2 fertilization effect (69 ± 12 Tg C year^{-1}) was comparable to the effect of LUCC.

The CO_2 fertilization effect was approximated by the Climate-CO_2 scenario minus the No-CO_2-Increase scenario (Fig. 3, A and E). For the 1985–2020 period, NPP, NEP, and NBP all increased by CO_2 fertilization, averaged at 160 ± 7, 93 ± 4.4, and 70 ± 4.1 Tg C, respectively. CO_2 fertilization increased biomass C stock by 1200 ± 120 Tg C and also increased soil C by 830 ± 26 Tg C. The CO_2 effect on C stock was mainly demonstrated in forested regions.

The Climate-CO_2 scenario minus the No-Climate-Change scenario indicates that the 1985–2020 climate trend led to an overall slight increase in NPP but did not affect NEP; however, both NPP and NEP demonstrated substantial annual variations. The Climate-CO_2 scenario had lower biomass C and soil C than the No-Climate-Change scenario mainly due to increased vegetation mortality and soil respiration, indicating that the actual climate trend reduced the overall C sink. At the CONUS scale, the cumulative differences in biomass and soil C were −210 ± 25 and −850 ± 58 Tg C, respectively, but these values varied spatially across the region (Fig. 3F). Actual climate during the past decade also led to intensified soil C loss (Fig. 3B). Climate variability reduced C stock of southeastern subtropical vegetation and western natural vegetation but increased C stock in the central CONUS. Climate effect was nonobvious on agricultural lands.

LUCC reduced terrestrial NPP, NEP, and NBP. Average differences of NPP, NEP, and NBP between the LUCC-Fire and the No-LUCC scenarios were −18.9 ± 2.9, −16.5 ± 2.9, and −68.0 ± 8.3 Tg C, respectively (Fig. 3C). LUCC led to a cumulative biomass C loss of −2200 ± 240 Tg C and a smaller soil C loss of −160 ± 22 Tg C. Spatially, LUCC-induced C losses were mostly in the southeastern and northwestern United States (Fig. 3G).

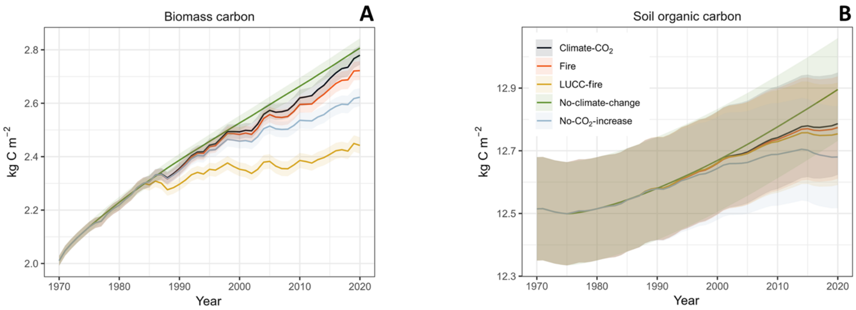

C

Scenario name	Increasing CO_2	Dynamic climate	Wildfire	LUCC
LUCC-Fire	Yes	Yes	Yes	Yes
Fire	Yes	Yes	Yes	No
Climate-CO_2	Yes	Yes	No	No
No-Climate-Change	Yes	No	No	No
No-CO_2-Increase	No	Yes	No	No

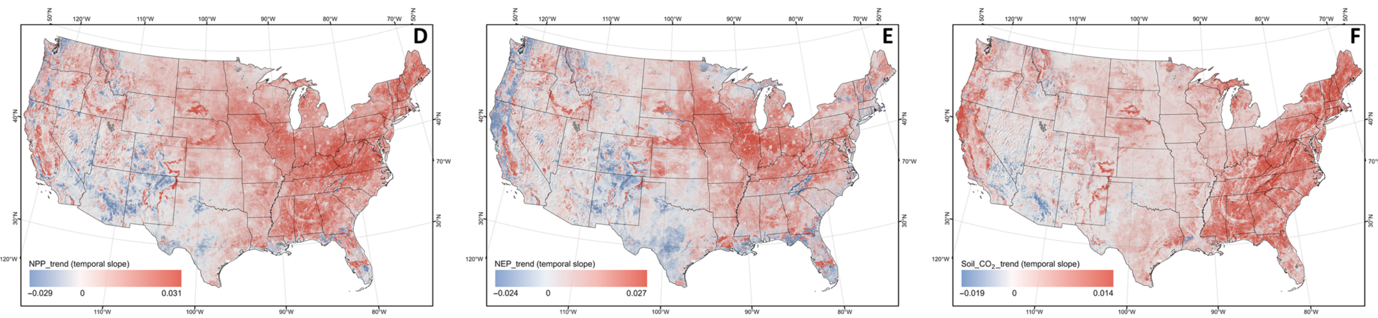

Fig. 2. Comparison of biomass and soil C stock changes across five scenarios and spatial patterns of C flux change. (**A** and **B**) Temporal trends of biomass and soil organic C under each scenario. (**C**) Scenario name and the inclusion (Yes) or exclusion (No) of driving factors. (**D** to **F**) Spatial patterns for the trends (linear regression slopes) of NPP, NEP, and soil respiration from 1985 to 2020 in the Climate-CO_2 scenario. Gray lines on maps are state boundaries.

Wildfire slightly reduced NPP but notably reduced NBP because of increasing wildfire magnitude and extent over time. Wildfires caused a cumulative biomass C loss of -450 ± 60 Tg C and soil C loss of -96 ± 8 Tg C over the 36 years compared to a no-fire condition (Fig. 3D). Fire effect mainly occurred in the Intermountain West and California (Fig. 3H). These estimates demonstrate that human land use and wildfire processes have notably reduced terrestrial C sink in CONUS during the study period.

Lateral C transport across landscapes and systems

The USPED simulation indicated that annually CONUS had 1800 Tg gross soil erosion and 1400 Tg gross soil deposition across terrestrial landscapes. The net soil erosion was 410 Tg year^{-1} (~50 Mg km^{-2} year^{-1}). The net soil C erosion, derived from pIBIS and assumed as particulate organic carbon (POC), averaged 8.8 ± 0.30 Tg C year^{-1} (~2% of eroded soil mass). Soil C leaching, originally included in pIBIS and assumed as dissolved organic carbon (DOC), was 30 ± 1.2 Tg C year^{-1}.

Soil ED had no effect on NPP but yielded lower NBP (-0.24 g C m^{-2} year^{-1}). Soil ED caused a minimal cumulative biomass C loss of -0.9 g C m^{-2}, or -7.2 Tg C (1 g C m^{-2} equals 7.8 Tg C for CONUS) but resulted in a substantial cumulative soil C loss of -33 g C m^{-2} (-260 Tg C) over 36 years. Spatially, high ED impacts mostly showed up near mountainous locations. Agricultural lands like the Corn Belt in central United States and the Central Valley of California showed low erosion effect (fig. S1).

Other C inputs to the aquatic system included human discharge from urban areas (1.0 Tg C year^{-1}), biologic DIC from soil respiration ($49 + 1.8$ Tg C year^{-1}), and geologic DIC from weathering processes (49 ± 1.1 Tg C year^{-1}). On the basis of average proportions of inland water C fluxes in the SOCCR2 (*9*), we estimated that CO_2 emissions from inland waters were 80 ± 1.9 Tg C year^{-1}, C burial was 19 ± 0.47 Tg C year^{-1}, and C export to coastal regions was 39 ± 0.95 Tg C year^{-1}.

The C deposition amount on CONUS coastal tidal wetlands and mudflats (i.e., elevations under 2 m and terrain slope close to 0) was estimated at 2.0 Tg C per year, which was included in our terrestrial NBP calculation.

Model performance

We calibrated the pIBIS model using regional observation data (i.e., forest biomass, vegetation growth rate, crop yield, deadwood, and MODIS NPP), as summarized in the County-scale model calibration section in Materials and Methods. We further compared our model results with various remote sensing, inventory, flux tower, and modeling studies. The C variables compared included biomass, litter, deadwood, and soil C stocks, as well as NPP, NEP, and aquatic C export. We also conducted model sensitivity tests and Monte Carlo simulations to quantify model uncertainty. Details are provided in the Supplementary Materials (figs. S2 to S8 and table S1).

Model comparisons with other studies indicate that current pIBIS estimates a lower C sink than previous studies (fig. S2), partly due to enhanced land cover change data usage and improved regional calibrations. The pIBIS C sink also shows a pattern very similar to the RECCAP2 (*5*) estimates.

Sensitivity tests (fig. S3) indicate that NPP allocation ratio to leaf and wood is a highly sensitive model parameter influencing both productivity and C stock. Increasing NPP allocation to leaf reduces NBP and C stock. The tree growth rate scalar (a modifier to NPP) is another sensitive parameter that higher scalar values lead to higher NBP and C stock. In addition, initial tree biomass C and the wood turnover ratio also affect NBP and C stock. Other factors are less sensitive.

The lateral C transport from terrestrial to aquatic system (erosion, leaching, DIC_bio, and DIC_geo) were summarized at the two-digit

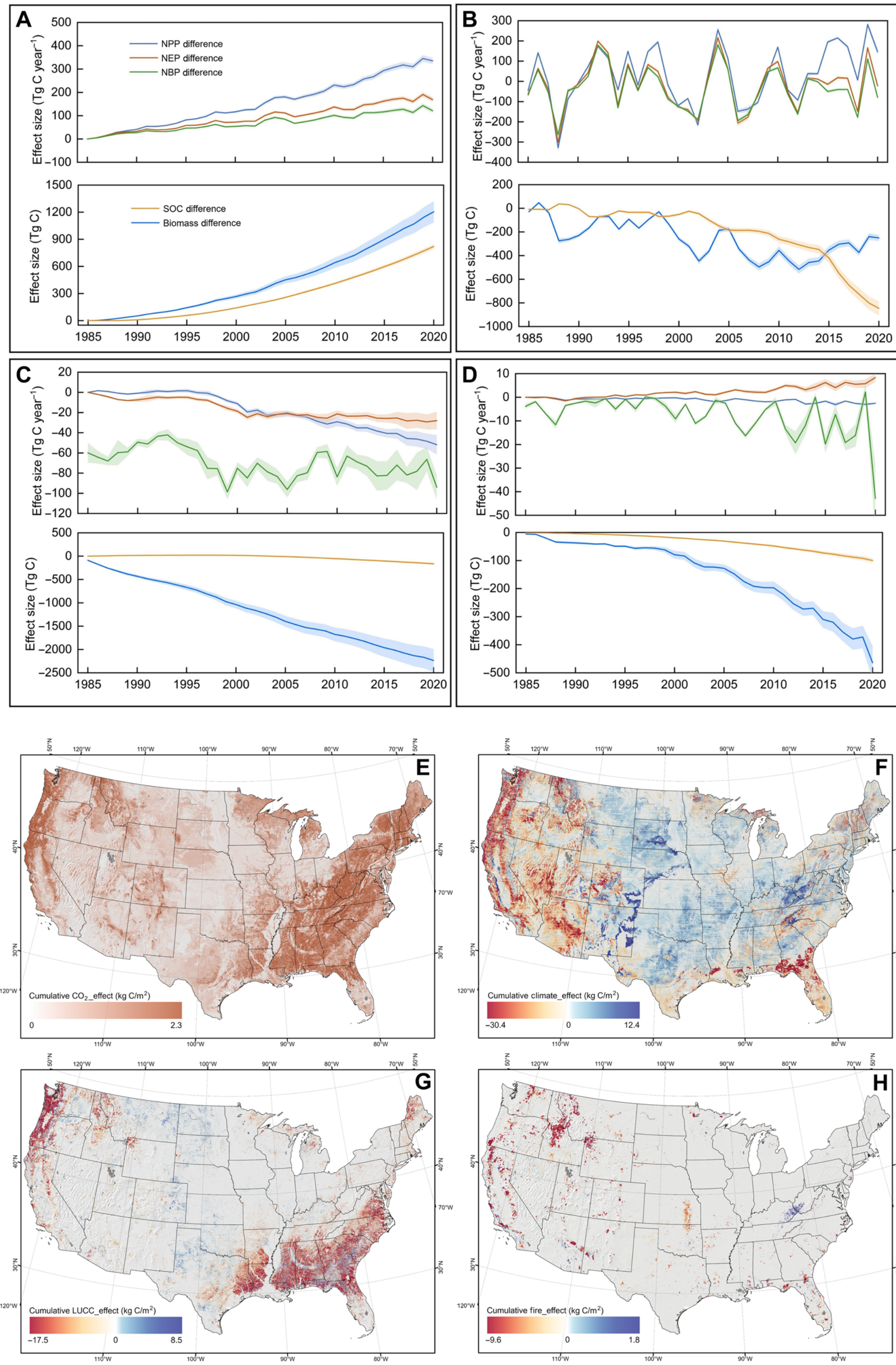

Fig. 3. Overall positive effect of CO_2 fertilization and negative effects of climate, LUCC, and wildfire on C stock change. Maps show the total ecosystem C difference between comparing scenarios. CO_2 effect is based on Climate-CO_2 minus NO-CO_2-Increase (**A** and **E**); climate effect is based on Climate-CO_2 minus No-Climate-Change (**B** and **F**); LUCC effect is based on LUCC-Fire minus Fire (**C** and **G**); wildfire effect is based on Fire minus Climate-CO_2 (**D** and **H**). SOC, soil organic carbon.

Hydrologic Unit Code (HUC level-2) watersheds in CONUS and were correlated with observed aquatic C data (R^2 around 0.2 to 0.4; figs. S4). The final CONUS-scale pIBIS estimate of lateral C export to coast (39 ± 0.95 Tg C year^{-1}) was close to the observed C export of 42 Tg C year^{-1} (*20*).

Temporal comparison of pIBIS NPP and MODIS NPP (*24*) at CONUS scale (fig. S5) indicates that they have the same temporal pattern. The overall pIBIS NPP was lower, partly because agricultural land in pIBIS did not incorporate MODIS NPP and grassland NPP was capped at 500 g C m^{-2} year^{-1}, which resulted in lower NPP estimates on the West Coast. However, forest NPP was of a similar magnitude because pIBIS NPP was calibrated using MODIS NPP.

The pIBIS wildfire C combustion was compared with data records from the Wildland Fire Emissions Information System (WFEIS) (fig. S6) (*25*). The pIBIS fire emission magnitude was about 37% lower than WFEIS because of differences in both fire area and burn severity level treatment.

Comparison of modeled 1-km NEP with data from the Harvard Forest flux tower indicates that pIBIS NEP is lower by about one-third to one-half (fig. S7). Flux tower data were adopted from Finzi *et al.* (*26*) and Curtis and Gough (*27*).

Spatial distribution of C stocks and NPP simulated by pIBIS is presented in fig. S8. Spatial correlation (Pearson correlation coefficient, r) of pIBIS variables with those from other studies is summarized in table S1. Forest NPP comparison has an r of 0.85, while All Lands NPP comparison has a lower r of 0.40. Spatial correlations between pIBIS C stocks and results from other studies indicate that forest live biomass C stock is highly corelated ($r = 0.86$ to 0.89) with NASA Carbon Monitoring System (CMS) (*28*) and Global C density data (*29*). Forest litter C and deadwood C show moderate correlations ($r = 0.66$ to 0.78), whereas forest soil C has a low correlation ($r = 0.46$ to 0.49) with CMS and Forest Inventory and Analysis (FIA) data (*30*).

DISCUSSION

Our results indicate a low and potentially weakening CONUS land C sink (terrestrial 110 ± 37 Tg C year^{-1} and aquatic 20 ± 0.47 Tg C year^{-1}) driven by C losses from human land use, wildfire, increased soil respiration, and lateral C transport, with implications for C sink size and C mitigation goals in the United States and beyond. We believe that many large-scale land C models have overestimated the CONUS terrestrial C sink. Our cross-scale modeling approach, using detailed land change data and regional calibration approaches, indirectly supports recent findings on the ocean C budget (suggesting that global ocean C sink has been underestimated) (*13*) and forest inventory data (indicating a decline in C sink strength since 1990) (*10*).

Our bottom-up study is robust in drawing the conclusion of a lower C sink than previous studies (refer to fig. S2). Our CONUS land C sink result was highest in the 1990s and showed two declining periods from 1992 to 2002 and from 2003 to 2020. Comparing our study with results from USEPA, USDA, SOCCR2, we found that pIBIS C results are close to forest inventory data, and in line with reported declines in forest C sequestration (refer to table S2) (*31*). SOCCR2 model projections suggested that North America C sink (2004 to 2013) has been relatively stable, except for the low-emission representative concentration pathway (RCP) 2.6 scenario, the net land C sinks of all other RCP scenarios would increase by mid-century and will either remain at current levels or notably decline thereafter (*9*). Similarly, relevant global C model synthesis (*1*, *17*) also estimate that global land C sink is being enhanced and would reach peak around mid-21st century. Our results suggest that the CONUS terrestrial C sink peaked in the 1990s and has not strengthened over the past four decades, with an increasing number of years exhibiting net C emissions since 2000 (refer to Table 1 and table S3).

We suggest that the discrepancy between our model and other DGVMs and ESMs is primarily due to differences in quantifying C sequestration and losses. Possible mechanisms include: (i) Fractional land cover change usage constrained NPP and C loss calculations. (ii) High rates of remote sensing–captured land change could have allowed more C loss in pIBIS. (iii) Missing C pools such as harvested wood product and landfills in pIBIS could have resulted in lower C sink estimates. (iv) Using only large fires (MTBS data) and likely low combustion ratios could have resulted in lower fire emissions. (v) Inclusion of C transport from land to aquatic system, like erosion consideration, could have reduced the C sink. Below are some detailed discussions on the similarity and difference between our results with other studies.

The pIBIS estimated NEP typically underpredict those measured by flux towers. This occurs because pIBIS uses coarser resolution (1 km) than plots and relies on averaged parameters (i.e., mixed vegetation cover, regional growth/mortality rates, and generic biomass, soil, and climate data) that do not match specific site conditions. Figure S7 shows the Harvard Forest flux tower (HA-1) measurements (*26*, *27*) compared to the pIBIS NEP on two test pixels, along with the inventory growth curve for the region. At the HA-1 site (characterized by mature, closed canopy, 80- to 120-year-old forest), live biomass C exceeds the regional median by about 22%. Total biomass C of the observed stand is about 25% higher than the regional average forest of the same age, which indicates that the forest stand had a higher growth rate than regional average. On the other hand, forest litter, deadwood, and soil C stocks may also contribute to the NEP difference. The HA-1 site measures soil C up to a depth of 45 cm, while pIBIS accounts for soil down to 2 m.

Although LUCC, fire, and climate change caused a slightly decreasing trend in C sink strength, the CO_2 fertilization could have increased NBP by 69 Tg C year^{-1} and increased CONUS total biomass C and soil C stock by 34 and 23 Tg C year^{-1}, respectively. Our model indicated an 11.3% in NPP with a corresponding 19% increase in atmospheric CO_2 (345 to 412 ppm) from 1985 to 2020. A recent field study on mature forest (*32*) indicated that CO_2 fertilization could lead to a 10.6% NPP increase when CO_2 increases by 36% (412 to 560 ppm). Our CO_2 effect on biomass C increase is 0.16% per year, about half of the recent forest inventory estimate of 0.3%, which was primarily derived from eastern US forests for the period of 1975 to 2015 (*33*). Because CO_2 fertilization effect at high CO_2 levels is assumed to be reduced because of progressive N limitation (*34*), our level of CO_2 effect is expected.

For soil C erosion, the previous 10-km resolution Energy Exascale Earth System Model study (*35*) suggested that CONUS net C erosion loss to inland water was about 14 Tg C year^{-1} from 1991 to 2012, mainly on croplands. This result is about 55% higher than our 1985–2020 1-km results, but the results are still comparable. Our high-erosion locations were not in cropland areas, although high geologic DIC yields were estimated on croplands.

We consider our results to be conservative, and we hypothesize that the CONUS C sink could be even lower than what we estimated in this study, especially with the inclusion of additional disturbance types and more small wildland fires. Incorporating structural changes to the representation of fine-root systems in pIBIS from the current prevailing single "big fine-root pool" with a more explicit multipool structure would invariably drive C sink estimates down even further. A recent study found that in temperate forests across the eastern United States, current ecosystem models with such a prevailing assumption of simple fine-root structure overestimate forest C sinks (*36*). Including more disturbance data like small wildfires and prescribed burnings (i.e., size <1000 acres for western United States and size <500 acres in eastern United States) and insect outbreaks would bring more accurate estimates of C losses. Last, detailed quantification of ecosystem aging effects, especially deadwood C accumulation and decomposition, could provide further understanding of the decreasing C sink. The increased ecosystem heterotrophic respiration could indicate a special ecosystem aging process under the climate change and disturbances: Over the 36 simulation years, both total biomass and tree biomass increased by only 6%, which does not indicate that forests had substantially grown older. However, deadwood C increased by 33%, which clearly indicates that the ecosystems were getting older in terms of deadwood C stock. This high deadwood C pool is the source of ecosystem C releases.

We acknowledge that some key aspects in the current pIBIS are not fully developed: Specifically, disturbances like hurricanes, insect kills, and major agricultural management activities are not accounted for in the model. Land cover types and land conversions considered in the model are fewer than the number of types available in the current remote sensing data (e.g., Annual NLCD has 16 land cover types). Site-scale calibration, such as using flux tower data, is challenging because the model mainly relies on coarse universal model parameters (refer to table S1). The current approach to simulating aquatic C is mainly based on inversion instead of physical bottom-up process. The current model still uses very simple biomass C pools (single leaf, single root, and single wood). Therefore, model improvements to these shortcomings, together with improved datasets, could refine CONUS C sink estimates to greater details.

Presently, the new generation of annual land cover products (e.g., Annual NLCD) provide more detailed vegetation and land use classes that could be used to better represent LUCC transitions that affect terrestrial C sinks. Increased temporal coverage could increase accuracies of C sink estimates at broad regional to national scales. Similarly, the FIA-COLE database facilitates the biomass growth calibration of pIBIS yet represents a simplified C calculation. New national-scale tree volume, biomass, and C modeling systems have recently been adopted in the US NFI (*21*). These methods will result in improved regional calibrations data for pIBIS and other DGVMs.

There has been a growing consensus that results from different C budget assessment methods (i.e., inversion, DGVM, inventory, and flux tower) are converging (*9*), but our results and those of other recent studies (*3*, *31*, *36*, *37*) do not support this consensus. Previous C modeling studies may have underestimated C losses due to limited land change data. If a convergence in C sink estimates emerges, we suggest that there could be a shift toward the lower range, especially with continued releases of higher spatial and temporal resolution LUCC data products and more detailed accounting of C flux components (e.g., ED). Also, deadwood C dynamics and lateral C transport remain substantial sources of uncertainty that could be reduced in large-scale C models but may require more new data collection across many regions.

Resolving the differences in land C sink estimates between top-down and bottom-up approaches could improve understanding of future land C sink potentials and attributions of land C fluxes. Our modeling approach represented detailed LUCC C fluxes over large regions. Moreover, our use of regional-scale inventory and census data to validate modeled C estimates increases overall model suitability and accuracy. The inclusion of cross-landscape, cross-system C transport further refines the C flux calculations. Our approach could be scaled up to larger spatial scales to fill in gaps between local- and global-scale models.

MATERIALS AND METHODS

Cross-scale modeling with the parallel IBIS and USPED

The IBIS v2 (*22*) has been modified and expanded into many variants by different modelers and scientists (*38*), including pIBIS. The overall processes considered in pIBIS is shown in Fig. 4. The pIBIS has several distinct modeling features: (i) Fine-resolution land cover data are used over large regions; (ii) process multiple fractional land cover changes are processed on each aggregated coarser resolution land pixel, usually beyond land management scale (e.g., 30 to 250 m); (iii) the model is calibrated using county-scale observed data; (iv) a high-resolution erosion model is linked with coarse resolution C model; and (v) a nonspatial inland water C accounting model is developed. Beyond that, the pIBIS included N feedback controls on C cycle, including controls on plant photosynthesis, C allocation, and soil organic C decomposition.

We demonstrate the cross-landscape and cross-system modeling features in our study. Cross-landscape modeling indicates the C movement between land pixels, which is quantified by the soil erosion model, while cross-system modeling indicates C transfer between terrestrial and aquatic systems. We calculate the amount of organic C lost from terrestrial to aquatic system by leaching (DOC) and erosion (POC), and the inorganic C yield from biologic source (DIC_bio) and geologic source (DIC_geo) partly based on inversion. We also quantify the amount of C deposited from sediments in water onto coastal tidal wetlands and mudflats. A portion of the aquatic C exported to coastal regions is deposited on tidal mudflats. This deposited C is considered a terrestrial C gain and is included in the terrestrial NBP. In contrast, C burial within inland water bodies is classified as an aquatic C gain. The sum of terrestrial and aquatic C gains represents the total land C gain or the total land NBP.

The pIBIS is a DGVM that has been enhanced to account for land disturbance processes (*2*). For this study, the model tracks C changes at 990-m resolution with 18 types of observed land conversions, 3 levels of wildfire severity, and soil C ED, all based on annual 30-m remote sensing products. Each 990-m land pixel can be a mixture of multiple cover types based on 30-m pixel aggregation. Annual land cover changes are expressed as fractional changes that happen simultaneously on individual land pixels, contrary to previous modeling that only allows one land disturbance event on a land pixel at one time step. The pIBIS model has been extensively developed for advanced computation, which enables it to run on Department of Energy exascale leadership class computers. Key model parameters and input data for pIBIS are listed in the Supplementary Materials.

The USPED model incorporates both soil ED, which is more favorable than traditional soil erosion models like the Universal Soil Loss Equation (USLE) and the Revised USLE that may have overestimated net soil erosion losses by not incorporating deposition (*39*).

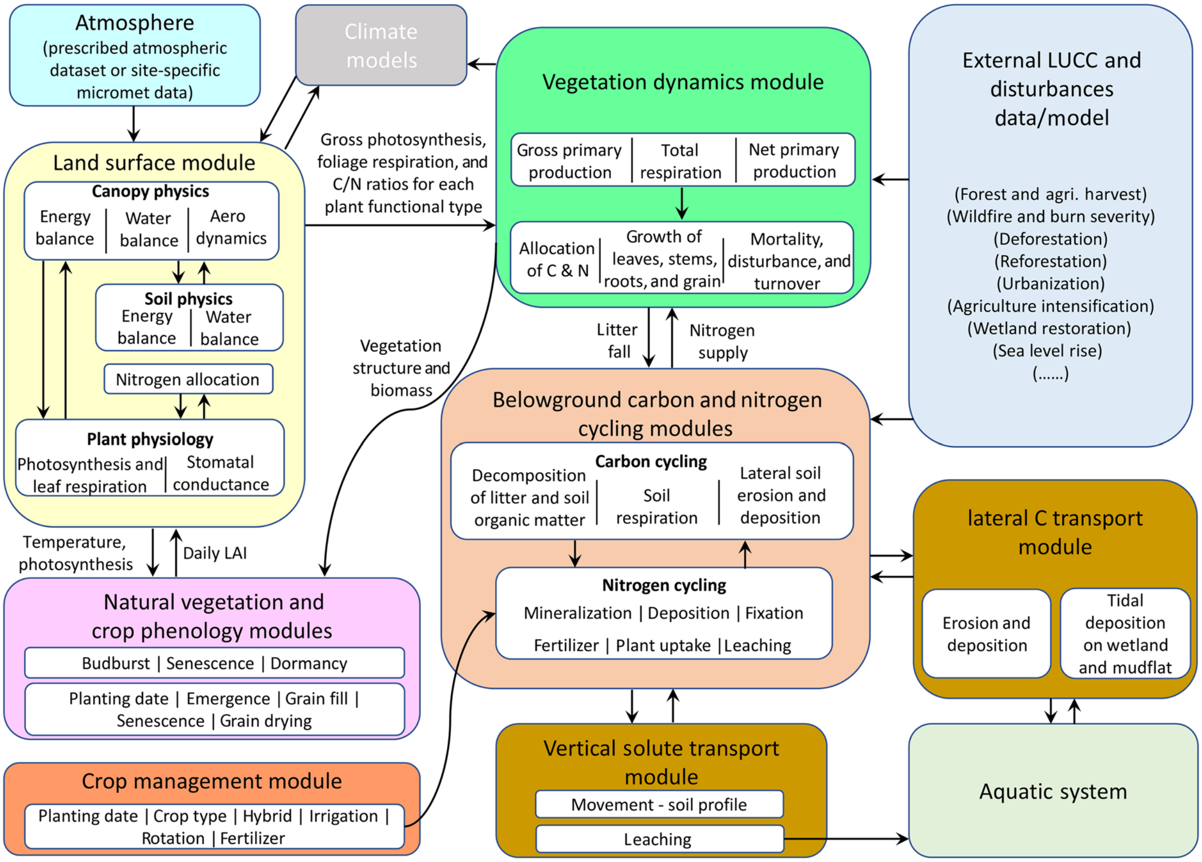

Fig. 4. Schematic diagram of the pIBIS. Flow chart was expanded with permission from Liu *et al.* (*38*).

The soil ED mainly depend on the sediment transport capacity of the surface runoff and is computed as a Two-dimensional divergence of sediment flow (https://ncsu-geoforall-lab.github.io/erosion-modeling-tutorial/erdep_theory.html). The USPED model needs four inputs: a digital elevation model (DEM), rainfall-runoff erosivity factor (R-factor), vegetation cover type (C-factor) and soil erodibility (K-factor) (*23*).

For the 90-m resolution annual USPED simulation across CONUS, we used the 1985–2020 4-km monthly PRISM precipitation data (*40*) to modify an 800-m resolution R-factor map (*41*), which quantifies the effects of raindrop impacts and reflects the amount and rate of runoff associated with the rain. The soil K-factor map (990 m, value 0 to 1) indicates the ease of soil detachment when raindrops hit the soil surface, which is only dependent on soil type and is available in the U.S. SURGGO soil database (*42*). The annual C-factor maps (90-m, value 0 to 1) indicate the soil export reduction effect of a given land cover type and were derived from LCMAP data resampled from 30 to 90 m (*43*). The 90-m NASA SRTM DEM (*44*) is used to calculate terrain aspect, slope, and flow accumulation.

The DEM and soil erodibility were assumed constant. Dynamic precipitation modified the R-factor annually. Dynamic land cover type determined the C-factor changes. The flow-accumulation calculation was also driven by land cover type with corresponding weighted values (*45*). USPED input data are shown in Fig. 5. Output 90-m soil ED values were aggregated to 990 m and constrained between −25 and +25 Mg ha^{-1} year^{-1}. Soil ED was translated to C ED when processed in pIBIS.

The USPED model is not suitable for land pixels with high flow accumulation values. High flow accumulation values directly lead to high erosion/deposition values. For the CONUS 90m USPED simulation, the extreme unrealistic ED values can reach −74 and +74 tons acre^{-1} year^{-1} (i.e., ±183 Mg ha^{-1} year^{-1}), respectively. Those extreme pixels are mostly located on or by river channels. Therefore, we separated the ED rates into two classes: normal and extreme. We put a cap of ±10 ton acre^{-1} (±24.7 Mg ha^{-1}) to define extreme erosion/deposition rates for those extreme pixels. Those extreme pixels occupy 3.8% of the total CONUS area, a little lower than the total inland water area (5.0% of CONUS), meaning that erosion/deposition on real land pixels (96.2% of CONUS area) are counted normally in UPSED; however, erosion/deposition on the extreme pixels (mostly shoreline or water pixels) are constrained with minimum and maximum values.

On the basis of literature, coastal tidal flat lands receive a substantial amount of sediment deposition from water. The USPED model cannot provide reasonable C deposition estimates on coastal tidal flat regions. Therefore, a global average rate of 130 g C m^{-2} year^{-1} (*46*) was adopted (inside the pIBIS model) to estimate the C deposition amount on coastal tidal flats, which describes the C transfer from aquatic system to land system by tidal dynamics. CONUS has about 14,000 km^2 coastal land with elevation below 2 m. Tidal mudflat area was comprised approximately 6477 km^2 (*47*).

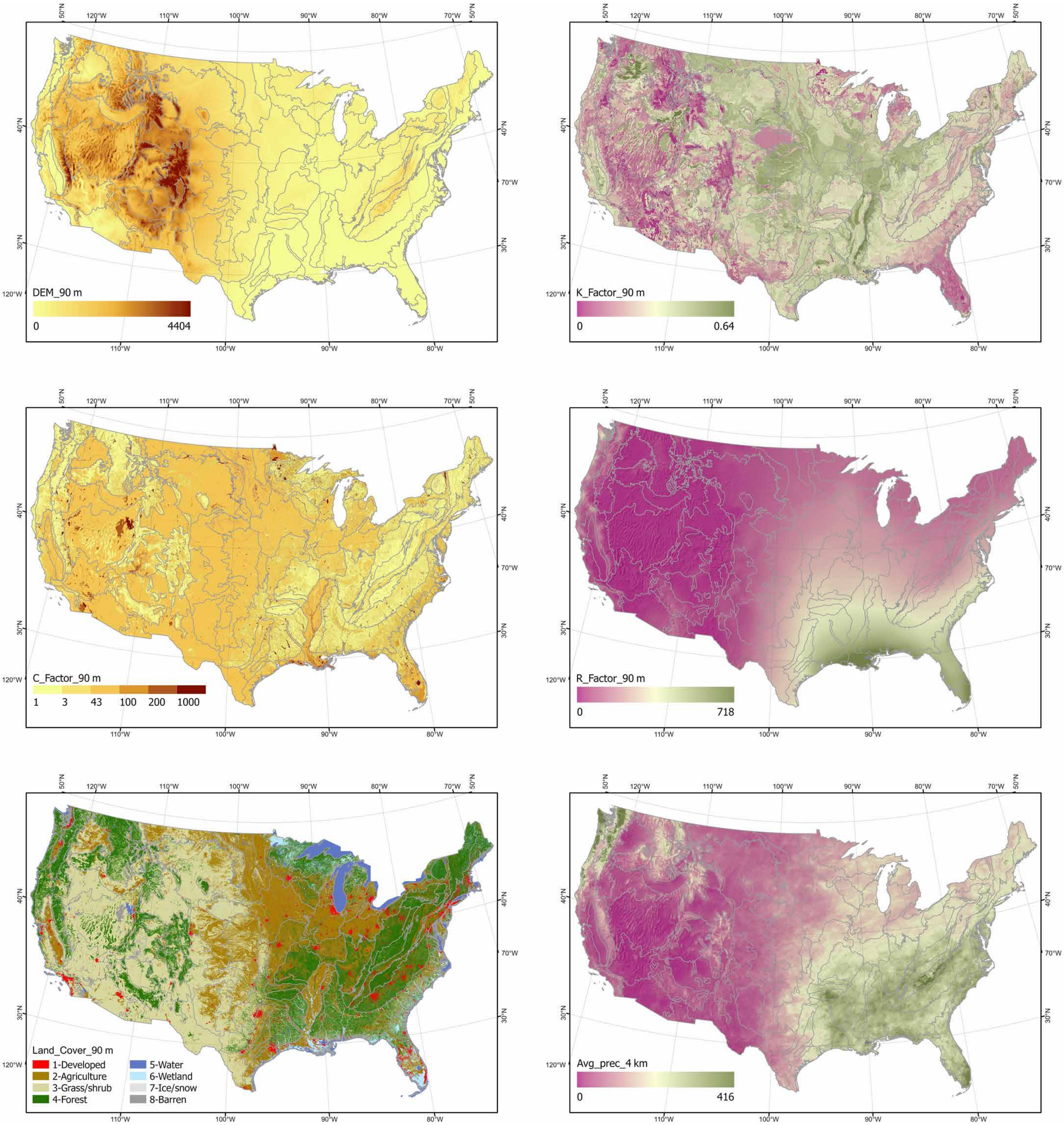

Fig. 5. USPED model 90-m input data. R-factor (800-m) has been resampled to 90-m resolution. Annual dynamic land cover (90-m) modifies the C-factor. Annual precipitation (4 km) modifies R-factor and surface water flow accumulation. Gray lines on maps are US EPA level-III ecoregion boundaries (*62*).

County-scale model calibration

The CONUS has 3111 counties. We performed county-scale model calibrations, in which MODIS-derived NPP (*48*), FIA-derived forest live biomass and deadwood (*49*), and USDA statistics of 1970–2009 crop yields were used (*50*). Calibration results are shown in Fig. 6.

The 1-km MODIS forest NPP of 2001–2005 was averaged at the county scale and compared with pIBIS county-scale forest NPP. An empirical scalar was added to NPP calculation to account for all the unknown environmental factors (e.g., species composition, age, and stem density). For crops, we used the county-scale crop yield of the 2000s to generate other empirical scalars, which partly reflect the effects of human activity in each county. The scalars were then used to modify the maximum Rubisco-limited rate of carboxylation (V_{max}) of related plant functional types (forest and crop) in the next pIBIS run. In addition to NPP and crop yield calibration, pIBIS-simulated forest total tree biomass and total deadwood C at 100 years were also calibrated with county-scale forest inventory summary using a biomass mortality scalar and a deadwood decomposition scalar.

Forest biomass and deadwood data were obtained from USDA Forest Service Carbon OnLine Estimator (COLE). The COLE application for live tree and standing dead C were obtained from a combination of FIA data and Resource Planning Assessment data, enhanced by other ecological data (*51*). The COLE application is no longer operable; however, the FIA data used in COLE relied on the component ratio method for live and standing dead C estimation (*16*), and those data are available at FIA Public data archive (*49*).

The simulated soil and litter C pools were not calibrated because of lack of regional data. However, we obtained a soil C balance for the period 1905–1984 with an accelerated soil spin-up and initialization approach (*52*) along with a soil C pool size derived from SURGGO database. The process was basically to compare the input and output fluxes of soil C pool. When input and output fluxes became very close, the soil C pool was close to a theoretical balanced state. To keep the overall soil C pool size close to the "observed" SURGGO soil C pool size, we dynamically adjust the slow and passive soil C pool sizes in the first 20 simulation years so that the total soil C size is still reasonable. There is no change of original IBIS soil C decomposition parameters.

The **p**IBIS is calibrated with FIA observed "regional" forest six FIA units. Each FIA unit has a COLE forest growth report, which usually contains dozens of tree species and hundreds of field plots. The pIBIS uses this 100-year growth curve to constrain forest regrowth. The growth curve covers both natural forest and plantations, all forest health condition, and wider canopy coverage fractions. The average

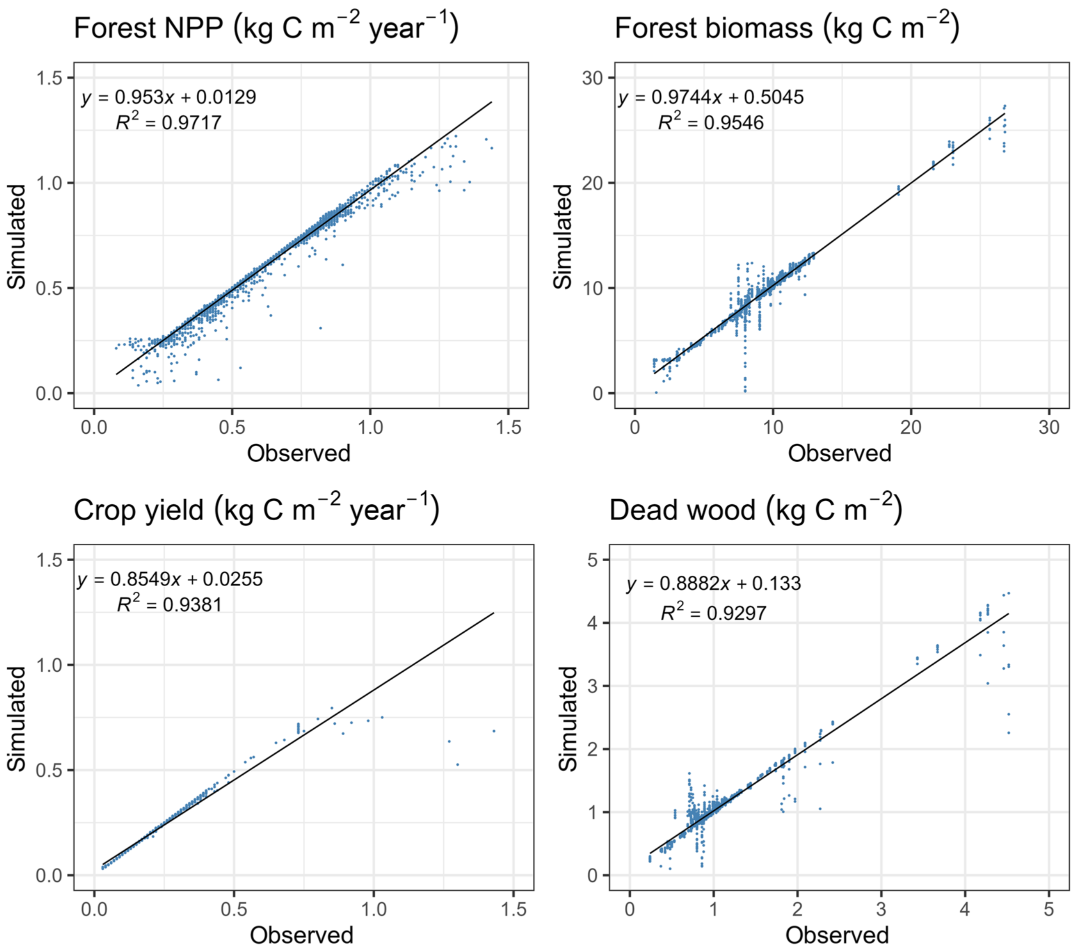

Fig. 6. Model calibrations at the county scale in CONUS. Observed annual NPP is based on the MODIS 2000–2005 NPP product (*48*). Observed live biomass and deadwood C in 100-year-old forests are derived the forest inventory database (*49*). Annual crop yield data (average of 29 species covering 1970 to 2009) are derived from the USDA NASS database (*50*).

forest live biomass and dead wood C stocks at age 100 for each of the 193 FIA units are provided in the Supplementary Materials.

A subset of COLE data for Alabama is illustrated in Fig. 7. The FIA units each have their pervasive sampling plots and specific average forest growth curve. Growth rate information of plantations (like loblolly pine, *Pinus taeda*) are also available. However, because of their relatively small area percentage, regional average forest growth curves are lower than the high-productive plantation growth curves (usually at young forest ages).

Thinning rates have been included in pIBIS, and the rates were allocated to each forest pixel each year, which adjusted the annual net tree biomass growth. The thinning rates for each county of eastern United States were derived from FIA database (*2*), and the thinning C amount is comparable to clearcut C amount if not more.

Fractional land cover change

The current pIBIS considers C processes among 6 land cover types and 18 land cover conversions, plus 2 non-land cover change events: (i) wildfire and (ii) harvest (Fig. 8) (*53*). Wildfire applies to all lands with independent wildfire input data. Harvest includes forest thinning and agricultural grain/straw removals, which are derived from forest inventory and agricultural census. Forest clearcut is represented by "Forest to Grassland" land cover conversion.

Summary of land change rates from the LCMAP data is shown in Fig. 9. We highlight the land cover change amount of forest to grassland and grassland to forest. The net forest area change was only about 10% of total forest area change. Most of the deforestation locations were later recovered to forest.

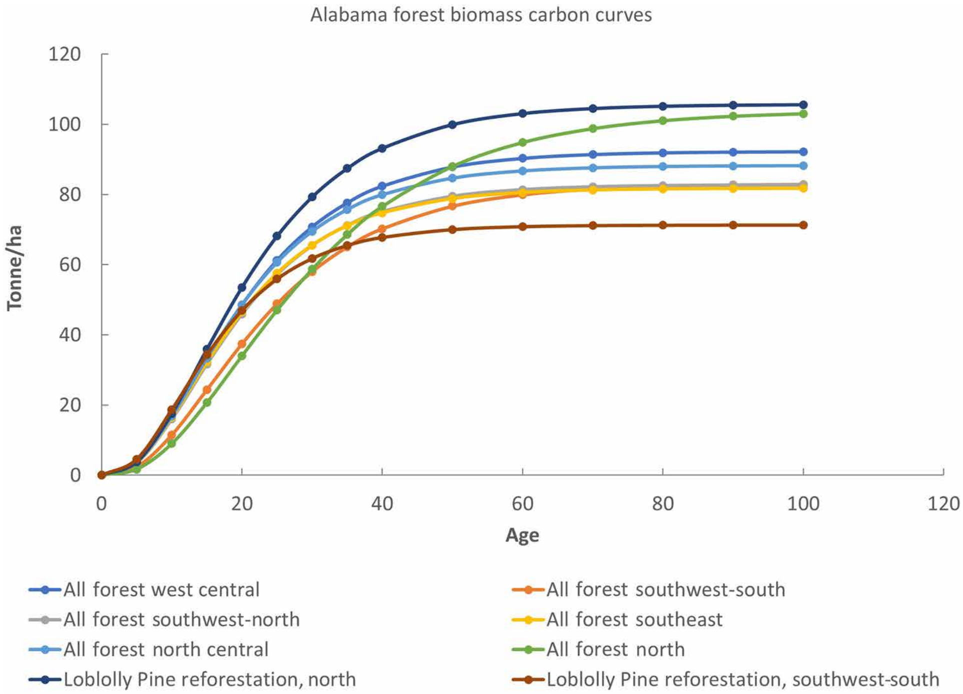

Fig. 7. Forest growth curves for Alabama. Each growth curve represents the average growth of multiple major tree species in a sub-subregion. The loblolly pine (*Pinus taeda*) growth curves represent a single tree species. Data were generated using the USDA Forest Service COLE with the forest inventory and analysis database (*49*).

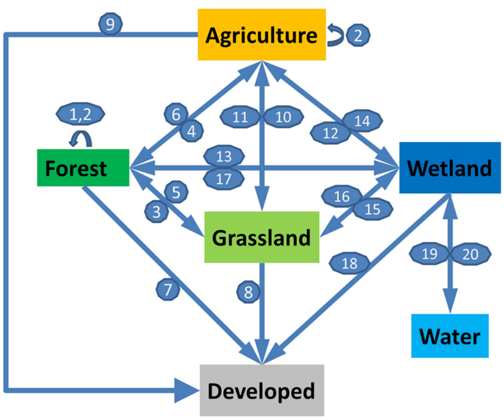

1	Fires	11	Agriculture to grassland
2	For. thinning and agri. harvest	12	Agriculture to wetland
3	Forest to grassland	13	Wetland to forest
4	Forest to agriculture	14	Wetland to agriculture
5	Grassland to tree cover	15	Grassland to wetland
6	Agriculture to forest	16	Wetland to grassland
7	Forest to developed	17	Forest to wetland
8	Grassland to developed	18	Wetland to developed
9	Agriculture to developed	19	Open water to wetland
10	Grassland to agriculture	20	Wetland to open water

Fig. 8. Land cover type and land change processes considered in the pIBIS model. The non-land change processes include wildfire (1) and tree partial cut and crop harvest (2). Chart was modified from Liu *et al.* (*53*) (CC BY-NC-ND; https://creativecommons.org/licenses/by-nc-nd/4.0/).

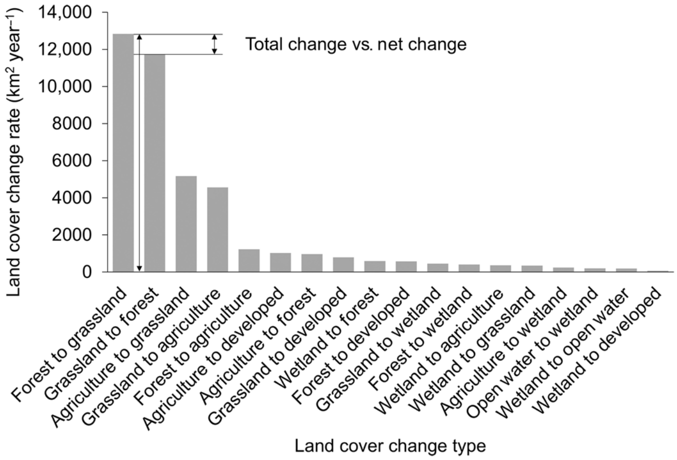

Fig. 9. Average CONUS land cover change rates from 1985 to 2020 summarized from LCMAP data (*43*). Amount indicates total or gross change. Net forest area change is only about 10% of total forest area change.

Inland water C accounting

C inputs to inland waters were based on both spatially explicit IBIS model simulation and additional data from literature. The amount of inland water C export to coast reported by Butman *et al.* (*20*) was calculated from observed USGS streamflow and water chemistry data (waterdata.usgs.gov/nwis) and was taken as an observed value for inversion. Organic C inputs from leaching through the soil profile and the erosion from soil surface were assumed to be DOC and POC, respectively. Additional C inputs from human residential discharge were calculated as a person's daily discharge [assumed 10 g C per person per day (*54*)] multiplied by increasing human population of CONUS. Aquatic photosynthesis process was not included.

The major inorganic C inputs, i.e., DIC from biologic source and geologic source, were derived on the basis of inversion, which totaled about 108 Tg C year^{-1}. We assumed that biologic DIC has links to soil respiration (soil CO_2 release) and daily drainage, while geologic DIC has links to exposed rock, sand, bare soil, and daily drainage. According to Stets *et al.* (*55*) and Zhong *et al.* (*56*), cropland would have higher DIC yield, and the ratio of riverine sources of geological CO_2 and biological CO_2 is close 1:1. Therefore, the daily DIC equations are formulated as

$$rDIC_{\mathrm{geo}} = A_0 * \left(0.5 - 0.25 * F_{\mathrm{Frac}} + A_{\mathrm{Frac}}\right) \tag{1}$$

$$DIC_{\mathrm{geo}} = 0.001 * rDIC_{\mathrm{geo}} * DDR \tag{2}$$

$$rDIC_{\mathrm{bio}} = B_0 * \left(0.5 + A_{\mathrm{Frac}}\right) \tag{3}$$

$$DIC_{\mathrm{bio}} = DSC * rDIC_{\mathrm{bio}} * DDR \ \ (\text{if } DDR \le 2 \text{ mm}) \tag{4}$$

$$DIC_{\mathrm{bio}} = DSC * rDIC_{\mathrm{bio}} * \left(2 + \frac{DDR - 2}{5}\right) \ (\text{if } DDR > 2 \text{ mm}) \tag{5}$$

where F_{Frac} and A_{Frac} are land cover fraction of forest and agricultural land, respectively; $A_0 = 1.0$ and $B_0 = 0.19$ are empirical ratios derived from inversion; DSC is daily soil CO_2 yield from soil respiration; DDR is daily drainage in millimeters per day.

Equations 1 and 2 demonstrate that calculated DIC_{geo} will increase with high agricultural land fraction and decrease with high forest cover fraction. Equations 3, 4, and 5 demonstrate that calculated DIC_{bio} will increase with high agricultural land fraction and high soil respiration but will be limited by daily drainage amount at high-drainage level.

The model parameter inversion was manually done with multiple simulations. With known aquatic DOC input (simulated from pIBIS) and known final aquatic C export (*20*), and following "law of mass balance," we calculated DIC input to aquatic system with assumptions built inside Eqs. 1 to 5. By adjusting equation constant ($A_0 = 1.0$ and $B_0 = 0.19$), we eventually matched simulated C export with observed data. The DIC calculations do not affect other pIBIS C outputs and were only obtained for the offline aquatic C calculation. We further derived the relative C flux magnitudes of CO_2 release (58%), burial (14%), and coastal export (28%) from the SOCRR2 Report (*9*) to differentiate aquatic fluxes.

Model parameters and input data

Selected model parameters are listed in table S4. Key model inputs of this study (refer to table S5) included 0.5° atmospheric chemistry data (CO_2 concentration and nitrogen deposition); 4-km monthly climate data (precipitation and temperature); 990-m annual land cover change fraction; wildfire burn severity, initial biomass, and soil erosion/deposition data aggregated from 30-m data sources; and 990-m soil texture and C data. All data were downscaled or aggregated to 990 m. The regional average 100-year forest growth curve data, derived from FIA, are provided in table S6.

1. The 1985–2020 990-m annual land cover fraction data were resampled from the 30-m LCMAP product classified using Landsat satellite imagery (*43*, *44*). We focused on 18 land change processes among 6 land cover classes (forest, grass, agriculture, urban, wetland, and open water) and built 18 land cover change maps each year with pixel values representing the fraction of changed 30-m pixels within the 990-m pixel. Together, 648 annual fractional LUCC maps were generated for 1985 to 2020. Each 990-m land pixel in the C model can have more than one cover type changes at each time step, which is different from many other models.

2. The 1985–2020 990-m annual wildfire disturbance data were resampled from the 30-m resolution MTBS data (*57*). The MTBS data include fires larger than 1000 acres in the western United States and fires larger than 500 acres in the eastern United States. More than 20,000 fires were included in this study. We used the MTBS burn severity levels (low, moderate, and high) to determine direct rates of wildfire combustion (for biomass, litter, and soil) and vegetation mortality.

3. Four-kilometer monthly precipitation and temperature data from 1976 to 2020 were obtained from the PRISM gridded monthly climatology (*40*).

4. The US SSURGO soil texture data around the year 2010 (*42*) was processed at 990-m resolution to represent soil profiles containing up to six layers (depth of up to 7, 15, 25, 50, 100, and 200 cm) with sand, silt, and clay fractions. Total soil organic C was also derived from SURRGO. The soil texture data are static and have biases

in bulk density in organic soils. Soil C data were used to initialize pIBIS and then were updated daily through the model.

5. The 990-m initial biomass maps were derived from the 30-m LANDFIRE vegetation cover and height data around 2000. The forest, shrub, and grass biomass maps were generated on the basis of a reference vegetation height-biomass look-up table and actual land cover fractions (*2*, *58*).

6. Monthly surface CO_2 concentrations (0.5°) were derived from satellite-based atmospheric CO_2 column density measurements made using the scanning imaging absorption spectrometer for atmospheric cartography (SCIAMACHY) of the ENVISAT (2003–2009) (*59*), which was used to spatially interpolate the global average CO_2 concentration from 1985 to 2020. Similarly, 0.5° annual N deposition maps (1970 to 2009), based on SCIAMACHY NO_2 column density and MOZART-4 model outputs, were generated to estimate recent spatially explicit rates of N deposition (refer to Supplementary Materials) (*60*).

7. The 1-km Protected Areas Database of the United States (PAD-US 4.0) (*61*) was used to separate protected lands from other private and production lands. Different forest thinning and forest regrowth adjustments were applied on protected lands and nonprotected lands.

Model sensitivity tests and Monte Carlo simulations

Tests of 10 model data/parameter factors on five output C variables were performed. Factors were tested at +10 and −10% on top of their base values. The 10 factors included

1) Initial forest biomass C
2) Initial shrub/grass biomass C
3) Initial soil organic C
4) Tree growth rate
5) Shrub growth rate
6) Grass growth rate
7) Woody biomass turnover rate
8) Litter turnover rate
9) Leaf C allocation ratio
10) Specific leaf area index

Their impacts on five C variables (NBP, NPP, NEP, biomass C, and soil C) were summarized in fig. S3. For those 10 factors, we also performed 40 Monte Carlo simulations at 10-km spatial resolution to quantify the approximate model uncertainty range. All factors are randomly assigned a value within 90 to 110% of its original value. The SD of each C variable was derived from the Monte Carlo runs. We used the 95% confidence level (1.96 * SD) to represent the model uncertainty range. However, the current Monte Carlo simulations did not cover parameters of agricultural system and aquatic system.

We combined several C variables into an auxiliary C variable for each Monte Carlo simulation, for example, *LUCC_removal* = *Live_C_removal* + *Dead_C_removal*, so that each auxiliary variable also had a Monte Carlo variation range. The auxiliary variables included *LUCC_removal*, *Fire_removal*, *Agri_removal*, *Mortality*, *All_litter*, and *All_aquatic_inputs*.

To analyze differences between two scenarios, each pair of Monte Carlo simulations (one from each scenario) produced one difference estimate. Thus, comparing two scenarios with 20 Monte Carlo simulations yielded 20 such estimates, which we used to describe the uncertainty associated with the scenario comparison. Monte Carlo–based model uncertainty ranges were reported in table S3.

Supplementary Materials

The PDF file includes:
Supplementary Text
Figs. S1 to S9
Tables S1 to S5
Legend for table S6
Data S1 to S10 (Available at USGS ScienceBase repository https://doi.org/10.5066/P1WDJOMS)
References

Other Supplementary Material for this manuscript includes the following:
Table S6

REFERENCES AND NOTES

1. P. Friedlingstein, M. O'Sullivan, M. W. Jones, R. M. Andrew, D. C. E. Bakker, J. Hauck, P. Landschützer, C. Le Quéré, I. T. Luijkx, G. P. Peters, W. Peters, J. Pongratz, C. Schwingshackl, S. Sitch, J. G. Canadell, P. Ciais, R. B. Jackson, S. R. Alin, P. Anthoni, L. Barbero, N. R. Bates, M. Becker, N. Bellouin, B. Decharme, L. Bopp, I. B. M. Brasika, P. Cadule, M. A. Chamberlain, N. Chandra, T. Chau, F. Chevallier, L. P. Chini, M. Cronin, X. Dou, K. Enyo, W. Evans, S. Falk, R. A. Feely, L. Feng, D. J. Ford, T. Gasser, J. Ghattas, T. Gkritzalis, G. Grassi, L. Gregor, N. Gruber, Ö. Gürses, I. Harris, M. Hefner, J. Heinke, R. A. Houghton, G. C. Hurtt, Y. Iida, T. Ilyina, A. R. Jacobson, A. Jain, T. Jarníková, A. Jersild, F. Jiang, Z. Jin, F. Joos, E. Kato, R. F. Keeling, D. Kennedy, K. K. Goldewijk, J. Knauer, J. I. Korsbakken, A. Körtzinger, X. Lan, N. Lefèvre, H. Li, J. Liu, Z. Liu, L. Ma, G. Marland, N. Mayot, P. C. McGuire, G. A. McKinley, G. Meyer, E. J. Morgan, D. R. Munro, S. Nakaoka, Y. Niwa, K. M. O'Brien, A. Olsen, A. M. Omar, T. Ono, M. Paulsen, D. Pierrot, K. Pocock, B. Poulter, C. M. Powis, G. Rehder, L. Resplandy, E. Robertson, C. Rödenbeck, T. M. Rosan, J. Schwinger, R. Séférian, T. Luke Smallman, S. M. Smith, R. Sospedra-Alfonso, Q. Sun, A. J. Sutton, C. Sweeney, S. Takao, P. P. Tans, H. Tian, B. Tilbrook, H. Tsujino, F. Tubiello, G. R. van der Werf, E. van Ooijen, R. Wanninkhof, M. Watanabe, C. Wimart-Rousseau, D. Yang, X. Yang, W. Yuan, X. Yue, S. Zaehle, J. Zeng, B. Zheng, Global carbon budget 2023. *Earth Syst. Sci. Data* **15**, 5301–5369 (2023).
2. J. Liu, B. M. Sleeter, Z. Zhu, T. R. Loveland, T. Sohl, S. M. Howard, C. H. Key, T. Hawbaker, S. Liu, B. Reed, M. A. Cochrane, L. S. Heath, H. Jiang, D. T. Price, J. M. Chen, D. Zhou, N. B. Bliss, T. Wilson, J. Sherba, Q. Zhu, Y. Luo, B. Poulter, Critical land change information enhances the understanding of carbon balance in the United States. *Glob. Chang. Biol.* **26**, 3920–3929 (2020).
3. Y. Wang, X. Wang, K. Wang, F. Chevallier, D. Zhu, J. Lian, Y. He, H. Tian, J. Li, J. Zhu, S. Jeong, J. G. Canadell, The size of the land carbon sink in China. *Nature* **603**, E7–E9 (2022).
4. J. P. Casas-Ruiz, P. Bodmer, K. A. Bona, D. Butman, M. Couturier, E. J. S. Emilson, K. Finlay, H. Genet, D. Hayes, J. Karlsson, D. Paré, C. Peng, R. Striegl, J. Webb, X. Wei, S. E. Ziegler, P. A. del Giorgio, Integrating terrestrial and aquatic ecosystems to constrain estimates of land-atmosphere carbon exchange. *Nat. Commun.* **14**, 1571 (2023).
5. B. Poulter, G. Murray-Tortarolo, D. J. Hayes, P. Ciais, R. M. Andrew, A. Bastos, B. Byrne, D. Butman, J. G. Canadell, A. Chatterjee, G. Domke, A. Feldman, K. Foster, N. Hunka, R. B. Jackson, W. A. Kurz, A. Lindquist, M. Liu, I. Luijkx, A. Mialon, A. M. Michalak, J. Miller, W. A. Obermeier, N. Pan, J. T. Randerson, P. A. Raymond, P. Regnier, L. Resplandy, G. Rocher-Ros, N. Rodriguez-Fernandez, J. Rosentreter, J. C. Salazar-Neira, S. E. Tank, H. Tian, R. Vargas, Y. Villalobos, J. A. Wang, X. Wei, K. P. Wickland, C. Williams, L. Windham-Myers, C. Woodall, Q. Ying, Z. Zhang, The North American greenhouse gas budget: Emissions, removals, and integration for CO_2, CH_4, and N_2O (2010–2019): Results from the Second REgional Carbon Cycle Assessment and Processes Study (RECCAP2). *Glob. Biogeochem. Cycles* **39**, e2024GB008310 (2025).
6. S. Ruehr, T. F. Keenan, C. Williams, Y. Zhou, X. Lu, A. Bastos, J. G. Canadell, I. C. Prentice, S. Sitch, C. Terrer, Evidence and attribution of the enhanced land carbon sink. *Nat. Rev. Earth Environ.* **4**, 518–534 (2023).
7. Y. Pan, R. A. Birdsey, O. L. Phillips, R. A. Houghton, J. Fang, P. E. Kauppi, H. Keith, W. A. Kurz, A. Ito, S. L. Lewis, G. Nabuurs, A. Shvidenko, S. Hashimoto, B. Lerink, D. Schepaschenko, A. Castanho, D. Murdiyarso, The enduring world forest carbon sink. *Nature* **631**, 563–569 (2024).
8. Intergovernmental Panel on Climate Change (IPCC), Climate Change 2022: Impacts, Adaptation and Vulnerability. Contribution of Working Group II to the Sixth Assessment Report of the Intergovernmental Panel on Climate Change, H.-O. Pörtner, D. C. Roberts, M. Tignor, E.S. Poloczanska, K. Mintenbeck, A. Alegría, M. Craig, S. Langsdorf, S. Löschke, V. Möller, A. Okem, B. Rama, Eds. (Cambridge Univ. Press, 2022), p. 3056. 10.1017/9781009325844.
9. USGCRP, Second State of the Carbon Cycle Report (SOCCR2): A Sustained Assessment Report, N. Cavallaro, G. Shrestha, R. Birdsey, M. A. Mayes, R. G. Najjar, S. C. Reed, P. Romero-Lankao, and Z. Zhu, Eds. (U.S. Global Change Research Program, Washington, DC, USA, 2018), p. 878. 10.7930/SOCCR2.2018.
10. G. M. Domke, B. F. Walters, J. E. Smith, E. J. Greenfield, C. L. Giebink, S. M. Ogle, J. Steller, K. Rewcastle, J. A. Knott, J. W. Coulston, K. A. Heilman, A. K. Lang, Greenhouse gas emissions

and removals from forest land, woodlands, urban trees, and harvested wood products in the United States, 1990–2022. *Resource Bulletin* WO-102 (Washington, DC: U.S. Department of Agriculture, Forest Service, Washington Office, 2024), p. 13.
11. J. Randerson, The weak land carbon sink hypothesis, in *2023 AGU Fall Meeting, Dec 11–15*; San Francisco. Abstract# GC54D-03. 2023AGUFMGC54D..03R (2023); https://agu.confex.com/agu/fm23/meetingapp.cgi/Paper/1412895.
12. A. P. Ballantyne, R. Andres, R. Houghton, B. D. Stocker, R. Wanninkhof, W. Anderegg, L. A. Cooper, M. DeGrandpre, P. P. Tans, J. C. Miller, C. Alden, J. W. C. White, Audit of the global carbon budget: Estimate errors and their impact on uptake uncertainty. *Biogeosci. Discuss.* **11**, 14929–14979 (2014).
13. A. J. Watson, U. Schuster, J. D. Shutler, T. Holding, I. G. C. Ashton, P. Landschützer, D. K. Woolf, L. Goddijn-Murphy, Revised estimates of ocean-atmosphere CO_2 flux are consistent with ocean carbon inventory. *Nat. Commun.* **11**, 4422 (2020).
14. R. C. Estoque, R. Dasgupta, K. Winkler, V. Avitabile, B. A. Johnson, S. W. Myint, Y. Gao, M. Ooba, Y. Murayama, R. D. Lasco, Spatiotemporal pattern of global forest change over the past 60 years and the forest transition theory. *Environ. Res. Lett.* **17**, 084022 (2022).
15. Y. Li, D. Sulla-Menashe, S. Motesharrei, X. Song, E. Kalnay, Q. Ying, S. Li, Z. Ma, Inconsistent estimates of forest cover change in China between 2000 and 2013 from multiple datasets: Differences in parameters, spatial resolution, and definitions. *Sci. Rep.* **7**, 8748 (2017).
16. J. A. Westfall, J. W. Coulston, G. G. Moisen, H.-E. Andersen, Sampling and estimation documentation for the Enhanced Forest Inventory and Analysis Program: 2022. General Technical Report NRS-GTR-207. Madison, WI: U.S. Department of Agriculture, Forest Service, Northern Research Station (2022), 129 p; https://doi.org/10.2737/NRS-GTR-207.
17. G. Murray-Tortarolo, B. Poulter, R. Vargas, D. Hayes, A. M. Michalak, C. Williams, L. Windham-Myers, J. A. Wang, K. P. Wickland, D. Butman, H. Tian, S. Sitch, P. Friedlingstein, M. O'Sullivan, P. Briggs, V. Arora, D. Lombardozzi, A. K. Jain, W. Yuan, R. Séférian, J. Nabel, A. Wiltshire, A. Arneth, S. Lienert, S. Zaehle, V. Bastrikov, D. Goll, N. Vuichard, A. Walker, E. Kato, X. Yue, Z. Zhang, A. Chaterjee, W. Kurz, A process-model perspective on recent changes in the carbon cycle of North America. *J. Geophys. Res. Biogeosci.* **127**, e2022JG006904 (2022).
18. G. C. Hurtt, L. Chini, R. Sahajpal, S. Frolking, B. L. Bodirsky, K. Calvin, J. C. Doelman, J. Fisk, S. Fujimori, K. Klein Goldewijk, T. Hasegawa, P. Havlik, A. Heinimann, F. Humpenöder, J. Jungclaus, J. O. Kaplan, J. Kennedy, T. Krisztin, D. Lawrence, P. Lawrence, L. Ma, O. Mertz, J. Pongratz, A. Popp, B. Poulter, K. Riahi, E. Shevliakova, E. Stehfest, P. Thornton, F. N. Tubiello, D. P. van Vuuren, X. Zhang, Harmonization of global land use change and management for the period 850–2100 (LUH2) for CMIP6. *Geosci. Model Dev.* **13**, 5425–5464 (2020).
19. K. Fennel, S. Alin, L. Barbero, W. Evans, T. Bourgeois, S. Cooley, J. Dunne, R. A. Feely, J. M. Hernandez-Ayon, X. Hu, S. Lohrenz, F. Muller-Karger, R. Najjar, L. Robbins, E. Shadwick, S. Siedlecki, N. Steiner, A. Sutton, D. Turk, P. Vlahos, Z. A. Wang, Carbon cycling in the North American coastal ocean: A synthesis. *Biogeosciences* **16**, 1281–1304 (2019).
20. D. Butman, S. Stackpoole, E. Stets, C. P. McDonald, D. W. Clow, R. G. Striegl, Aquatic carbon cycling in the conterminous United States and implications for terrestrial carbon accounting. *Proc. Natl. Acad. Sci. U.S.A.* **113**, 58–63 (2016).
21. J. A. Westfall, J. W. Coulston, A. N. Gray, J. D. Shaw, P. J. Radtke, D. M. Walker, A. R. Weiskittel, D. W. MacFarlane, D. L.R. Affleck, D. Zhao, H. Temesgen, K. P. Poudel, J. M. Frank, S. P. Prisley, Y. Wang, A. J. Sánchez Meador, D. Auty, G. M. Domke, A national-scale tree volume, biomass, and carbon modelling system for the United States. Gen. Tech. Rep. WO-104 (Washington, DC: U.S. Department of Agriculture, Forest Service, 2024), p. 60.
22. C. J. Kucharik, J. A. Foley, C. Delire, V. A. Fisher, M. T. Coe, J. D. Lenters, C. Young-Molling, N. Ramankutty, J. M. Norman, S. T. Gower, Testing the performance of a dynamic global ecosystem model: Water balance, carbon balance, and vegetation structure. *Global Biogeochem. Cycles* **14**, 795–825 (2000).
23. H. Mitasova, J. Hofierka, M. Zlocha, L. R. Iverson, Modelling topographic potential for erosion and deposition using GIS. *Int. J. Geogr. Inf. Syst.* **10**, 629–641 (1996).
24. Google, Earth Engine Data Catalog, https://developers.google.com/earth-engine/datasets/catalog/MODIS_061_MOD17A3HGF. [accessed 27 November 2024].
25. N. H. F. French, D. McKenzie, T. Erickson, B. Koziol, M. Billmire, K. A. Endsley, N. K. Y. Scheinerman, L. Jenkins, M. E. Miller, R. Ottmar, S. Prichard, Modeling regional-scale fire emissions with the Wildland Fire Emissions Information System. *Earth Interact.* **18**, 1–26 (2014).
26. A. C. Finzi, M.-A. Giasson, A. A. Barker Plotkin, J. D. Aber, E. R. Boose, E. A. Davidson, M. C. Dietze, A. M. Ellison, S. D. Frey, E. Goldman, T. F. Keenan, J. M. Melillo, J. William Munger, K. J. Nadelhoffer, S. V. Ollinger, D. A. Orwig, N. Pederson, A. D. Richardson, K. Savage, J. Tang, J. R. Thompson, C. A. Williams, S. C. Wofsy, Z. Zhou, D. R. Foster, Carbon budget of the Harvard Forest Long-Term Ecological Research site: Pattern, process, and response to global change. *Ecological monographs* **90**, e01423 (2020).
27. P. S. Curtis, C. M. Gough, Forest aging, disturbance and the carbon cycle. *New Phytol.* **219**, 1188–1193 (2018).
28. Y. Yu, S. S. Saatchi, B. F. Walters, S. Ganguly, S. Li, S. Hagen, L. Melendy, R. R. Nemani, G.M. Domke, C.W. Woodall, Carbon Pools across CONUS using the MaxEnt Model, 2005, 2010, 2015, 2016, and 2017 (ORNL DAAC, Oak Ridge, Tennessee, USA, 2021); https://doi.org/10.3334/ORNLDAAC/1752; https://daac.ornl.gov/cgi-bin/dsviewer.pl?ds_id=1752. [accessed 12 December 2024].
29. S. A. Spawn, H. K. Gibbs, Global Aboveground and Belowground Biomass Carbon Density Maps for the Year 2010. (ORNL DAAC, Oak Ridge, Tennessee, USA, 2020); https://doi.org/10.3334/ORNLDAAC/1763. [accessed 12 December 2024].
30. B. Cao, G. M. Domke, M. B. Russell, B. F. Walters, Spatial modeling of litter and soil carbon stocks on forest land in the conterminous United States. *Sci. Total Environ.* **654**, 94–106 (2019).
31. D. Wear, J. Coulston, From sink to source: Regional variation in U.S. forest carbon futures. *Sci. Rep.* **5**, 16518 (2015).
32. R. J. Norby, N. J. Loader, C. Mayoral, S. Ullah, G. Curioni, A. R. Smith, M. K. Reay, K. van Wijngaarden, M. Shoaib Amjad, D. Brettle, M. E. Crockatt, G. Denny, R. T. Grzesik, R. Liz Hamilton, K. M. Hart, I. P. Hartley, A. G. Jones, A. Kourmouli, J. R. Larsen, Z. Shi, R. M. Thomas, A. Robert MacKenzie, Enhanced woody biomass production in a mature temperate forest under elevated CO_2. *Nat. Clim. Change* **14**, 983–988 (2024).
33. J. A. Hogan, G. M. Domke, K. Zhu, D. J. Johnson, J. W. Lichstein, Climate change determines the sign of productivity trends in US forests. *Proc. Natl. Acad. Sci. U.S.A.* **121**, e2311132121 (2024).
34. Y. Luo, B. Su, W. S. Currie, J. S. Dukes, A. Finzi, U. Hartwig, B. Hungate, R. E. McMurtrie, R. Oren, W. J. Parton, D. E. Pataki, R. M. Shaw, D. R. Zak, C. B. Field, Progressive nitrogen limitation of ecosystem responses to rising atmospheric carbon dioxide. *Bioscience* **54**, 731–739 (2004).
35. Z. Tan, L. R. Leung, H. Li, T. Tesfa, Q. Zhu, M. Huang, A substantial role of soil erosion in the land carbon sink and its future changes. *Glob. Change Biol.* **26**, 2642–2655 (2020).
36. B. Wang, M. L. McCormack, D. M. Ricciuto, X. Yang, C. M. Iversen, Embracing fine-root system complexity in terrestrial ecosystem modeling. *Glob. Chang. Biol.* **29**, 2871–2885 (2023).
37. J. Wang, L. Feng, P. I. Palmer, Y. Liu, S. Fang, H. Bösch, C. W. O'Dell, X. Tang, D. Yang, L. Liu, C. Xia, Large Chinese land carbon sink estimated from atmospheric carbon dioxide data. *Nature* **586**, 720–723 (2020).
38. J. Liu, X. Lu, Q. Zhu, W. Yuan, Q. Yuan, Z. Zhang, Q. Guo, C. Deering, Terrestrial ecosystem modelling with IBIS: Progress and future vision. *J. Resour. Ecol.* **13**, 2–16 (2022).
39. S. W. Trimble, P. Crosson, U.S. soil erosion rates: Myth and reality. *Science* **289**, 248–250 (2000).
40. PRISM Climate Group, Oregon State University, https://prism.oregonstate.edu, [accessed December 2022].
41. K. G. Renard, C. R. Foster, G. A. Weesies, D. K. McCool, D. C. Yoder, Predicting Soil Erosion by Water: A Guide to Conservation Planning with the Revised Universal Soil Loss Equation (RUSLE). U.S. Department of Agriculture, Agriculture Handbook Number 703, (Government Printing Office, Washington, DC, 1997), pp. 47–51, https://ntrl.ntis.gov/NTRL/dashboard/searchResults/titleDetail/PB97153704.xhtml.
42. Soil Survey Staff, Natural Resources Conservation Service, United States Department of Agriculture. Web Soil Survey, https://websoilsurvey.nrcs.usda.gov. [accessed December 2009].
43. J. F. Brown, H. J. Tollerud, C. P. Barber, Q. Zhou, J. L. Dwyer, J. E. Vogelmann, T. R. Loveland, C. E. Woodcock, S. V. Stehman, Z. Zhu, B. W. Pengra, K. Smith, J. A. Horton, G. Xian, R. F. Auch, T. L. Sohl, K. L. Sayler, A. L. Gallant, D. Zelenak, R. R. Reker, J. Rover, Lessons learned implementing an operational continuous United States national land change monitoring capability: The Land Change Monitoring, Assessment, and Projection (LCMAP) approach. *Remote Sens. Environ.* **238**, 111356 (2020).
44. NASA Shuttle Radar Topography Mission (SRTM) (2013), Shuttle Radar Topography Mission (SRTM) Global. Distributed by OpenTopography; https://doi.org/10.5069/G9445JDF. [accessed 22 December 2022].
45. J. Liu, S. Liu, L. L. Tieszen, M. Chen, Estimating Soil Erosion Using the USPED Model and Consecutive Remotely Sensed Land Cover Observations, in Proceedings of the 2007 Summer Simulation Multiconference (SCSC'07). The Society for Modelling and Simulation International, San Diego, USA, July 2007 (2007). CD ROM. Available online at http://sce.carleton.ca/faculty/wainer/SCSC07/SCSC%2707.htm; https://dl.acm.org/doi/abs/10.5555/1357910.1358122.
46. Z. L. Chen, Y. L. Shing, Tidal flats as a significant carbon reservoir in global coastal ecosystems. *Front. Mar. Sci.* **9**, 900896 (2022).
47. N. J. Murray, S. R. Phinn, M. DeWitt, R. Ferrari, R. Johnston, M. B. Lyons, N. Clinton, D. Thau, R. A. Fuller, The global distribution and trajectory of tidal flats. *Nature* **565**, 222–225 (2019).
48. M. Zhao, F. A. Heinsch, R. R. Nemani, S. W. Running, Improvements of the MODIS terrestrial gross and net primary production global data set. *Remote Sens. Environ.* **95**, 164–176 (2005).
49. USDA Forest Service (2023). Forest Inventory and Analysis Database: FIADB_1.9.0.02_ARCHIVE, https://usfs-public.app.box.com/s/e9qmctjeekurhu5p8gfrtuk2n28q8yje/folder/227953849375. [accessed 10 July 2025].

50. U.S. National Agricultural Statistics Service (NASS), Quick Stats Agricultural Database. https://quickstats.nass.usda.gov/. [accessed December 2012.
51. M. P. Spinney, P. C. Van Deusen, L. S. Heath, J. E. Smith, 2005. COLE: Carbon on-line estimator, Version 2, in *Changing Forests - Challenging Times: Proceedings of the New England Society of American Foresters 85th Winter Meeting; 2005 March 16-18*, L. S. Kenefic, M. J. Twery, eds. General Technical Report NE-325. (Newtown Square, PA: U.S. Department of Agriculture, Forest Service, Northeastern Research Station: 28, 2005).
52. J. Y. Xia, Y. Q. Luo, Y.-P. Wang, E. S. Weng, O. Hararuk, A semi-analytical solution to accelerate spin-up of a coupled carbon and nitrogen land model to steady state. *Geosci. Model Dev.* **5**, 1259–1271 (2012).
53. J. Liu, B. Sleeter, P. C. Selmants, J. Diao, Q. Zhou, B. Worstell, M. Moritsch, Modeling watershed carbon dynamics as affected by land cover change and soil erosion. *Ecol. Model.* **459**, 109724 (2021).
54. C. Rose, A. Parker, B. Jefferson, E. Cartmell, The characterization of feces and urine: A review of the literature to inform advanced treatment technology. *Crit. Rev. Environ. Sci. Technol.* **45**, 1827–1879 (2015).
55. E. G. Stets, R. G. Striegl, K. P. Wickland, M. Dornblaser, S. Foks, Dissolved carbon export by large river systems is influenced by source area heterogeneity. *Global Biogeochem. Cycles* **37**, e2022GB007392 (2023).
56. J. Zhong, S. Li, F. Tao, F. Yue, C. Liu, Sensitivity of chemical weathering and dissolved carbon dynamics to hydrological conditions in a typical karst river. *Sci. Rep.* **7**, 42944 (2017).
57. Z. Zhu (editor), B. Bergamaschi, R. Bernknopf, D. Clow, D. Dye, S. Faulkner, W. Forney, R. Gleason, T. Hawbaker, J. Liu, S. Liu, S. Prisley, B. Reed, M. Reeves, M. Rollins, B. Sleeter, T. Sohl, S. Stackpoole, S. Stehman, R. Striegl, A. Wein, Z. Zhu, A method for assessing carbon stocks, carbon sequestration, and greenhouse-gas fluxes in ecosystems of the United States under present conditions and future scenarios: U.S. Geological Survey Scientific Investigations Report 2010–5233, 188 p. (2010); http://pubs.usgs.gov/sir/2010/5233.
58. LANDFIRE, Existing Vegetation Type Layer, LANDFIRE 1.1.0, U.S. Department of the Interior, Geological Survey (2008). https://landfire.gov/viewer/; https://landfire.gov/data, [accessed 28 October 2010].
59. Z. Zhang, H. Jiang, J. Liu, X. Zhang, C. Huang, X. Lu, J. Jin, G. Zhou, An analysis of the global spatial variability of column-averaged CO_2 from SCIAMACHY and its implications for CO_2 sources and sinks. *Int. J. Remote Sens.* **35**, 2047–2066 (2014).
60. X. Lu, H. Jiang, J. Liu, X. Zhang, J. Jin, Q. Zhu, Z. Zhang, C. Peng, Simulated effects of nitrogen saturation on the global carbon budget using the IBIS model. *Sci. Rep.* **6**, 39173 (2016).
61. U.S. Geological Survey (USGS) Gap Analysis Project (GAP), Protected Areas Database of the United States (PAD-US) 4.0: U.S. Geological Survey data release (2024) https://doi.org/10.5066/P96WBCHS. [accessed August 2024].
62. U.S. Environmental Protection Agency, 1999. Level III Ecoregions of the Continental United States, (1:7,500,000-scale map). Corvallis, Oregon: U.S. Environmental Protection Agency, National Health and Environmental Effects Research Laboratory. https://www.epa.gov/eco-research/level-iii-and-iv-ecoregions-continental-united-states.
63. G. M. Domke, B. F. Walters, C. L. Giebink, E. J. Greenfield, J. E. Smith, M. C. Nichols, J. A. Knott, S. M. Ogle, J. W. Coulston, J. Steller. Greenhouse gas emissions and removals from forest land, woodlands, urban trees, and harvested wood products in the United States, 1990–2021. Resour. Bull. WO-101 (Washington, DC: U.S. Department of Agriculture, Forest Service, Washington Office, 2023), 10 p. https://doi.org/10.2737/WO-RB-101.
64. U.S. Environmental Protection Agency (EPA), Greenhouse Gas Inventory Data Explorer, https://cfpub.epa.gov/ghgdata/inventoryexplorer/#landuse/entiresector/allgas/category/all. [accessed July 2024].
65. Z. Zhu, D. McGuire, eds., Baseline and projected future carbon storage and greenhouse-gas fluxes in ecosystems of Alaska: U.S. Geological Survey Professional Paper 1826, p. 196. (2016); http://dx.doi.org/10.3133/pp1826.
66. Intergovernmental Panel on Climate Change (IPCC), 2019 Refinement to the 2006 IPCC Guidelines for National Greenhouse Gas Inventories, E. Calvo Buendia, K. Tanabe, A. Kranjc, J. Baasansuren, M. Fukuda, S. Ngarize, A. Osako, Y. Pyrozhenko, P. Shermanau, S. Federici, Eds. (IPCC, Switzerland, 2019); https://www.ipcc.ch/report/2019-refinement-to-the-2006-ipcc-guidelines-for-national-greenhouse-gas-inventories/.
67. W. Zhou, K. Guan, B. Peng, A. Margenot, D. Lee, J. Tang, Z. Jin, R. Grant, E. DeLucia, Z. Qin, M. M. Wander, S. Wang, How does uncertainty of soil organic carbon stock affect the calculation of carbon budgets and soil carbon credits for croplands in the U.S. Midwest? *Geoderma* **429**, 116254 (2023).
68. B. M. Sleeter, T. L. Sohl, T. R. Loveland, R. F. Auch, W. Acevedo, M. A. Drummond, K. Sayler, S. V. Stehman, Land-cover change in the conterminous United States from 1973 to 2000. *Glob. Environ. Change* **23**, 733–748 (2013).
69. J. Eidenshink, B. Schwind, K. Brewer, Z. Zhu, B. Quayle, S. Howard, A project for monitoring trends in burn severity. *Fire Ecol.* **3**, 3–21 (2007).
70. LANDFIRE, 2016, Existing vegetation type layer, LANDFIRE 2.0.0, U.S. Department of the Interior, Geological Survey, and U.S. Department of Agriculture; https://www.landfire.gov/viewer/ [accessed 28 April 2017].
71. NOAA Office for Coastal Management, Coastal Change Analysis Program (C-CAP) High-Resolution Land Cover. Charleston, SC: NOAA Office for Coastal Management; https://coastalimagery.blob.core.windows.net/ccap-landcover/CCAP_bulk_download/index.html [accessed August 2022].
72. B. M. Sleeter, P. C. Selmants, Carbon stocks and fluxes for the conterminous United States 2001-2020: U.S. Geological Survey data release (2022); https://doi.org/10.5066/P9QUIRNP.
73. C. Potter, S. Klooster, A. Huete, V. Genovese, Terrestrial carbon sinks for the United States predicted from MODIS satellite data and ecosystem modeling. *Earth Interact.* **11**, 1–21 (2007).
74. D. J. Hayes, D. P. Turner, G. Stinson, A. D. McGuire, Y. Wei, T. O. West, L. S. Heath, B. de Jong, B. G. McConkey, R. A. Birdsey, W. A. Kurz, A. R. Jacobson, D. N. Huntzinger, Y. Pan, W. Mac Post, R. B. Cook, Reconciling estimates of the contemporary North American carbon balance among terrestrial biosphere models, atmospheric inversions, and a new approach for estimating net ecosystem exchange from inventory-based data. *Glob. Chang. Biol.* **18**, 1282–1299 (2012).
75. S. W. Pacala, G. C. Hurtt, D. Baker, P. Peylin, R. A. Houghton, R. A. Birdsey, L. Heath, E. T. Sundquist, R. F. Stallard, P. Ciais, P. Moorcroft, J. P. Caspersen, E. Shevliakova, B. Moore, G. Kohlmaier, E. Holland, M. Gloor, M. E. Harmon, S.-M. Fan, J. L. Sarmiento, C. L. Goodale, D. Schimel, C. B. Field, Consistent Land- and Atmosphere-Based U.S. Carbon Sink Estimates. 2001 VOL 292 SCIENCE; https://science.org/doi/10.1126/science.1057320.
76. F. Deng, J. M. Chen, M. Ishizawa, C. Yuen, G. Mo, K. Higuchi, D. Chan, S. Maksyutov, Global monthly CO_2 flux inversion with a focus over North America. *Tellus* **59**, 179–190 (2022).
77. P. B. Woodbury, J. E. Smith, L. S. Heath, Carbon sequestration in the U.S. forest sector from 1990 to 2010. *For. Ecol. Manage.* **241**, 14–27 (2007).

Acknowledgments

Funding: This work was supported by the USGS Land Change Science Program. B.W. was supported by the DOE-BER Earth & Environmental Systems Modeling (EESM) Program under contract DE-AC05-00OR22725. Early funding for this work was also provided by the DOD ESTCP Program (RC 201703, to J.L. and B.M.S.) and by the NASA Interdisciplinary Sciences (NNX11AB89G, to M.A.C. and J.L.). This research used resources of the DOE Leadership Computing Facilities, which is a DOE Office of Science User Facility supported under contract DE-AC02-06CH11357 and DE-AC02-05CH11231, using NERSC ward ALCC-ERCAP0022618 (to J.L., C.E.S., B.M.S., and Q. Zhu). **Author contributions:** Writing—original draft: J.L., P.C.S., M.A.C., R.G.S., T.J.H., T.L.S., T.S.W., and Z. Zhang, Conceptualization: B.M.S., B.W., E.J.W., J.L., K.P.W., L.W.-M., M.A.C., R.G.S., T.J.H., T.S.W., and Z. Zhu. Investigation: B.W., G.M.D., J.L., K.P.W., Q. Zhu, T.L.S., and Z. Zhu. Writing—review and editing: All authors. Methodology: B.W., E.J.W., G.M.D., J.L., K.P.W., L.W.-M., R.G.S., T.J.H., T.L.S., T.S.W., and Q. Zhu. Resources: B.M.S., B.W., C.E.S., G.M.D., Q. Zhou, and Z. Zhang. Data curation: G.M.D., J.L., L.W.-M., and P.C.S. Validation: B.W., E.J.W., G.M.D., and J.L. Formal analysis: B.W., J.L., Q. Zhou, P.C.S., R.G.S., and Z. Zhu. Software: J.L. and Q. Zhou. Project administration: J.L. and Z. Zhu. Visualization: J.L., P.C.S., and T.S.W. Funding acquisition: B.M.S. and M.A.C. Supervision: B.M.S. **Competing interests:** The authors declare that they have no competing interests. **Data and materials availability:** All data needed to evaluate the conclusions in the paper are present in the paper and/or the Supplementary Materials. Additional data and pIBIS model code are available through the USGS ScienceBase repository (https://doi.org/10.5066/P1WDJOMS). The pIBIS model code is also available on Github: https://github.com/jxliu2018/pIBIS and Zenodo: https://zenodo.org/records/17135663. Any use of trade, firm, or product names is for descriptive purposes only and does not imply endorsement by the US government. Further, the findings and conclusions in this publication are those of the author(s) and should not be construed to represent any official US Department of Agriculture or US government determination or policy.

Submitted 28 March 2025
Accepted 25 September 2025
Published 12 November 2025
10.1126/sciadv.adx7823